

Benchmarking the Robustness of Semantic Segmentation Models

Christoph Kamann and Carsten Rother

Visual Learning Lab

Heidelberg University (HCI/IWR)

<http://vislearn.de>

Abstract

When designing a semantic segmentation module for a practical application, such as autonomous driving, it is crucial to understand the robustness of the module with respect to a wide range of image corruptions. While there are recent robustness studies for full-image classification, we are the first to present an exhaustive study for semantic segmentation, based on the state-of-the-art model DeepLabv3+. To increase the realism of our study, we utilize almost 400,000 images generated from Cityscapes, PASCAL VOC 2012, and ADE20K. Based on the benchmark study, we gain several new insights. Firstly, contrary to full-image classification, model robustness increases with model performance, in most cases. Secondly, some architecture properties affect robustness significantly, such as a Dense Prediction Cell, which was designed to maximize performance on clean data only.

1. Introduction

In recent years, Deep Convolutional Neural Networks (DCNN) have set the state-of-the-art on a broad range of computer vision tasks [50, 37, 74, 76, 53, 67, 11, 29, 36, 52]. The performance of DCNN models is generally measured using benchmarks of publicly available datasets, which often consist of clean and post-processed images [18, 24]. However, it has been shown that model performance is prone to image corruptions [90, 78, 39, 27, 23, 28, 3], especially image noise decreases the performance significantly.

Image quality depends on environmental factors such as illumination and weather conditions, ambient temperature, and camera motion since they directly affect the optical and electrical properties of a camera. Image quality is also affected by optical aberrations of the camera lenses, causing, e.g., image blur. Thus, in safety-critical applications, such as autonomous driving, models must be robust towards such inherently present image corruptions [34, 48, 46].

In this work, we present an extensive evaluation of the robustness of semantic segmentation models towards a broad range of real-world image corruptions. Here, the term *robustness* refers to training a model on clean data and

then validating it on corrupted data. We choose the task of semantic image segmentation for two reasons. Firstly, image segmentation is often applied in safety-critical applications, where robustness is essential. Secondly, a rigorous evaluation for real-world image corruptions has, in recent years, only been conducted for full-image classification and object detection, e.g., most recently [27, 39, 59].

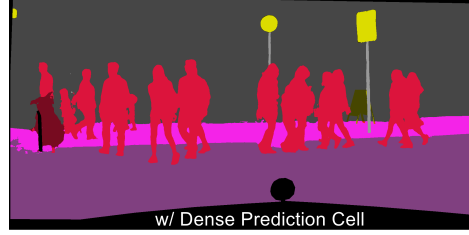
When conducting an evaluation of semantic segmentation models, there are, in general, different choices such as: i) comparing different architectures, or ii) conducting a detailed ablation study of a state-of-the-art architecture. In contrast to [27, 39], which focused on aspect i), we perform both options. We believe that an ablation study (option ii) is important since knowledge about architectural choices are likely helpful when designing a practical system, where types of image corruptions are known beforehand. For example, [27] showed that ResNet-152 [37] is more robust to image noise than GoogLeNet [76]. Is the latter architecture more prone to noise due to missing skip-connections, shallower architecture, or other architectural design choices? When the overarching goal is to develop robust DCNN models, we believe that it is important to learn about the robustness capabilities of architectural properties.

We conduct our study on three popular datasets: Cityscapes [18], PASCAL VOC 2012 [24], and ADE20K [88, 89]. To generate a wide-range of image corruptions, we utilize the image transformations presented by Hendrycks *et al.* [39]. While they give a great selection of image transformations, the level of realism is rather lacking, in our view. Hence we augment their image transformations by additional ones, in particular, intensity-dependent camera noise, PSF blur, and geometric distortions. In total, we employ 19 different image corruptions from the categories of blur, noise, weather, digital, and geometric distortion. We are thus able to validate each DCNN model on almost 400,000 images.

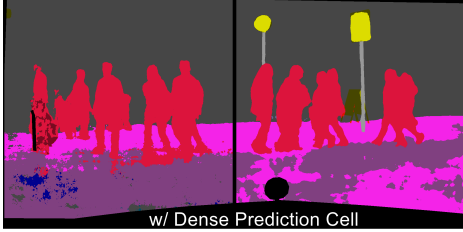
We use the state-of-the-art DeepLabv3+ architecture [14] with multiple network backbones as reference and consider many ablations of it. Based on our evaluation, we are able to conclude two main findings: 1) Contrary to the task of full-image classification, we observe that the ro-



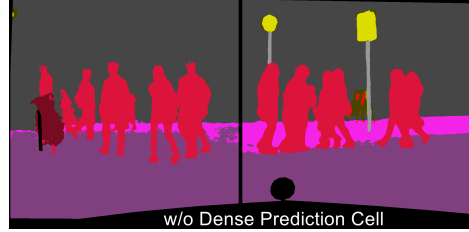
(a) Corrupted validation image (left: noise, right: blur)



(b) Prediction of best-performing architecture on clean image



(c) Prediction of best-performing architecture on corrupted image



(d) Prediction of ablated architecture on corrupted image

Figure 1: Results of our ablation study. Here we train the state-of-the-art semantic segmentation model DeepLabv3+ on clean Cityscapes data and test it on corrupted data. (a) A validation image from Cityscapes, where the left-hand side is corrupted by *shot noise* and the right-hand side by *defocus blur*. (b) Prediction of the best-performing model-variant on the corresponding clean image. (c) Prediction of the same architecture on the corrupted image (a). (d) Prediction of an ablated architecture on the corrupted image (a). We clearly see that prediction (d) is superior to (c), hence the corresponding model is more robust with respect to this image corruption. We present a study of various architectural choices and various image corruptions for the three datasets Cityscapes, PASCAL VOC 2012, and ADE20K.

business of semantic segmentation models of DeepLabv3+ increases often with model performance. 2) Architectural properties can affect the robustness of a model significantly. Our results show that atrous (i.e., dilated) convolutions and long-range link naturally aid the robustness against many types of image corruptions. However, an architecture with a Dense Prediction Cell [10], which was designed to maximize performance on clean data, hampers the performance for corrupted images significantly (see Fig. 1).

In summary, we give the following contributions:

- We benchmark the robustness of many architectural properties of the state-of-the-art semantic segmentation model DeepLabv3+ for a wide range of real-world image corruptions. We utilize almost 400,000 images generated from the Cityscapes dataset, PASCAL VOC 2012, and ADE20K.
- Besides DeepLabv3+, we have also benchmarked a wealth of other semantic segmentation models.
- We develop a more realistic noise model than previous approaches.
- Based on the benchmark study, we have several new insights: 1) contrary to full-image classification, model robustness of DeepLabv3+ increases with model performance, in most cases; 2) Some architecture properties affect robustness significantly.

2. Related Work

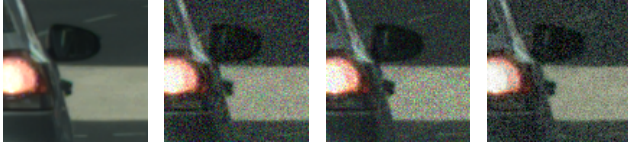
Robustness studies [90, 78, 39, 27, 22, 23, 61, 59] and robustness enhancement [82, 87, 29, 40, 7, 75, 26] of DCNN

architectures [50, 76, 74, 71, 56, 11, 12, 14, 13, 60, 5] have been addressed in various benchmarks [24, 18, 21]. Recent work also dealt with evaluating and increasing the robustness of CNNs against various weather conditions [68, 79, 20, 15, 69]. Vasiljevic *et al.* [78] examined the impact of blur on full-image classification and semantic segmentation using VGG-16 [74]. Model performance decreases with an increased degree of blur for both tasks. We also focus in this work on semantic segmentation but evaluate on a much wider range of real-world image corruptions.

Geirhos *et al.* [27] compared the generalization capabilities of humans and Deep Neural Networks (DNNs). The ImageNet dataset [21] is modified in terms of color variations, noise, blur, and rotation.

Hendrycks *et al.* [39] introduce the “ImageNet-C dataset”. The authors corrupted the ImageNet dataset by common image corruptions. Although the absolute performance scores increase from AlexNet [50] to ResNet [37], the robustness of the respective models does barely change. They further show that Multigrid and DenseNet architectures [49, 43] are less prone to noise corruption than ResNet architectures. In this work, we use most of the proposed image transformations and apply them to the Cityscapes dataset, PASCAL VOC 2012, and ADE20K [18, 24, 88, 89].

Geirhos *et al.* [26] showed that humans and DNNs classify images with different strategies. Unlike humans, DNNs trained on ImageNet seem to rely more on local texture instead of global object shape. The authors then show that model robustness w.r.t. image corruptions increases, when CNNs rely more on object shape than on object texture.



(a) Clean image (b) Gaussian (c) Shot (d) Proposed
Figure 2: A crop of a validation image from Cityscapes corrupted by various noise models. (a) Clean image. (b) Gaussian noise. (c) Shot noise. (d) Our proposed noise model. The amount of noise is high in regions with low pixel intensity.

Robustness of models with respect to adversarial examples is an active field of research [44, 6, 17, 31, 9, 58, 8]. Arnab *et al.* [2] evaluate the robustness of semantic segmentation models for adversarial attacks of a wide variety of network architectures (e.g. [86, 4, 63, 85, 84]). In this work, we adopt a similar evaluation procedure, but we do not focus on the robustness w.r.t. adversarial attacks, which are typically not realistic, but rather on physically realistic image corruptions. We further rate robustness w.r.t. many architectural properties instead of solely comparing CNN architectures. Our approach modifies a single property per model at a time, which allows for an accurate evaluation.

Ford *et al.* [28] connect adversarial robustness and robustness with respect to image corruption of Gaussian noise. The authors showed that training procedures that increase adversarial robustness also improve robustness with respect to many image corruptions.

3. Image Corruption Models

We evaluate the robustness of semantic segmentation models towards a broad range of image corruptions. Besides using image corruptions from the ImageNet-C dataset, we propose new and more realistic image corruptions.

3.1. ImageNet-C

We employ many image corruptions from the ImageNet-C dataset [39]. These consist of several types of *blur*: motion, defocus, frosted glass and Gaussian; *Noise*: Gaussian, impulse, shot and speckle; *Weather*: snow, spatter, fog, and frost; and *Digital*: brightness, contrast, and JPEG compression. Each corruption is parameterized with five severity levels. We refer to the supplemental material for an illustration of these corruptions.

3.2. Additional Image Corruptions

Intensity-Dependent Noise Model. DCNNs are prone to noise. Previous noise models are often simplistic, e.g., images are evenly distorted with Gaussian noise. However, *real* image noise significantly differs from the noise generated by these simple models. Real image noise is a combination of multiple types of noise (e.g., photon noise, kTC noise, dark current noise as described in [38, 83, 57, 55]).

We propose a noise model that incorporates commonly observable behavior of cameras. Our noise model consists of two noise components: i) a chrominance and luminance noise component, which are both added to original pixel intensities in linear color space. ii) an intensity-level dependent behavior. In accordance with image noise observed from real-world cameras, pixels with low intensities are noisier than pixels with high intensities. Fig. 2 illustrates noisy variants of a Cityscapes image-crop. In contrast to the other, simpler noise models, the amount of noise generated by our noise model depends clearly on pixel intensity.

PSF blur. Every optical system of a camera exhibits aberrations, which mostly result in image blur. A point-spread-function (PSF) aggregates all optical aberrations that result in image blur [47]. We denote this type of corruption as *PSF blur*. Unlike simple blur models, such as Gaussian blur, real-world PSF functions are spatially varying. We corrupt the Cityscapes dataset with three different PSF functions that we have generated with the optical design program *Zemax*, for which the amount of blur increases with a larger distance to the image center.

Geometric distortion. Every camera lens exhibits geometric distortions [25]. We applied several radially-symmetric barrel distortions [80] as a polynomial of grade 4 [73] to both the RGB-image and respective ground truth.

4. Models

We employ DeepLabv3+ [14] as the reference architecture. We chose DeepLabv3+ for several reasons. It supports numerous network backbones, ranging from novel state-of-art models (e.g., modified aligned Xception [16, 14, 66], denoted by *Xception*) and established ones (e.g., ResNets [37]). For semantic segmentation, DeepLabv3+ utilizes popular architectural properties, making it a highly suitable candidate for an ablation study. Please note that the range of network backbones, offered by DeepLabv3+, represents different execution times since different applications have different demands.

Besides DeepLabv3+, we have also benchmarked a wealth of other semantic segmentation models, such as FCN8s [56], VGG-16 [74], ICNet [85], DilatedNet [84], ResNet-38 [81], PSPNet [86], and the recent Gated-ShapeCNN (GSCNN) [77].

4.1. DeepLabv3+

Fig. 3 illustrates important elements of the DeepLabv3+ architecture. A network backbone (ResNet, Xception or MobileNet-V2) processes an input image [37, 70, 42]. Its output is subsequently processed by a multi-scale processing module, extracting dense feature maps. This module is either Dense Prediction Cell [10] (DPC) or Atrous Spatial Pyramid Pooling (ASPP, with or without global average pooling (GAP)). We consider the variant with ASPP and

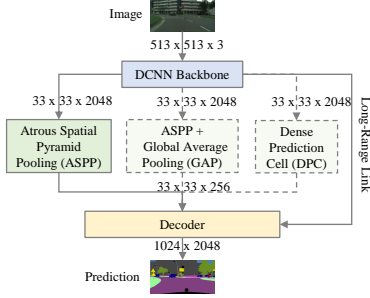


Figure 3: Building blocks of DeepLabv3+. Input images are firstly processed by a network backbone, containing atrous convolutions. The backbone output is further processed by a multi-scale processing module (ASPP or DPC). A long-range link concatenates early features of the network backbone with encoder output. Finally, the decoder outputs estimates of semantic labels. Our reference model is shown by regular arrows (*i.e.*, without DPC and GAP). The dimension of activation volumes is shown after each block.

without GAP as reference architecture. A long-range link concatenates early features from the network backbone with features extracted by the respective multi-scale processing module. Finally, the decoder outputs estimates of the semantic labels.

Atrous convolution. Atrous (*i.e.*, dilated) convolution [12, 41, 62] is a type of convolution that integrates spacing between kernel parameters and thus increases the kernel field of view. DeepLabv3+ incorporates atrous convolutions in the network backbone.

Atrous Spatial Pyramid Pooling. To extract features at different scales, several semantic segmentation architectures [12, 11, 86] perform Spatial Pyramid Pooling [35, 30, 51]. DeepLabv3+ applies Atrous Spatial Pyramid Pooling (ASPP), where three atrous convolutions with large atrous rates (6, 12 and 18) process the DCNN output.

Dense Prediction Cell. [10] is an efficient multi-scale architecture for dense image prediction, constituting an alternative to ASPP. It is the result of a neural-architecture-search with the objective to maximize the performance for clean images. In this work, we analyze whether this objective leads to overfitting.

Long-Range link. A long-range link concatenates early features of the encoder with features extracted by the respective multi-scale processing module [32]. In more detail, for Xception (MobileNet-V2) based models, the long-range link connects the output of the second or the third Xception block (inverted residual block) with ASPP or DPC output. Regarding ResNet architectures, the long-range link connects the output of the second residual block with the ASPP or DPC output.

Global Average Pooling. A global average pooling (GAP) layer [54] averages the feature maps of an activation volume. DeepLabv3+ incorporates GAP in parallel to the ASPP.

4.2. Architectural Ablations

In the next section, we evaluate various ablations of the DeepLabv3+ reference architecture. In detail, we remove atrous convolutions (AC) from the network backbone by transforming them into regular convolutions. We denote this ablation in the remaining sections as w/o AC. We further removed the long-range link (LRL, *i.e.*, w/o LRL) and Atrous Spatial Pyramid Pooling (ASPP) module (w/o ASPP). The removal of ASPP is additionally replaced by Dense Prediction Cell (DPC) and denoted as w/o ASPP+ w/o DPC. We also examined the effect of global average pooling (w/o GAP).

5. Experiments

We present the experimental setup (sec. 5.1) and then the results of two different experiments. We firstly benchmark multiple neural network backbone architectures of DeepLabv3+ and other semantic segmentation models (sec. 5.2). While this procedure gives an overview of the robustness across several architectures, no conclusions about which architectural properties affect the robustness can be drawn. Hence, we modify multiple architectural properties of DeepLabv3+ (sec. 4.2) and evaluate the robustness for re-trained ablated models w.r.t. image corruptions (sec. 5.3, 5.4, 5.5). Our findings show that architectural properties can have a substantial impact on the robustness of a semantic segmentation model w.r.t. image corruptions.

5.1. Experimental Setup

Network backbones. We trained DeepLabv3+ with several network backbones on clean and corrupted data using TensorFlow [1]. We utilized MobileNet-V2, ResNet-50, ResNet-101, Xception-41, Xception-65 and Xception-71 as network backbones. Every model has been trained with batch size 16, crop-size 513×513 , fine-tuning batch normalization parameters [45], initial learning rate 0.01 or 0.007, and random scale data augmentation.

Datasets. We use PASCAL VOC 2012, the Cityscapes dataset, and ADE20K for training and validation. The training set of PASCAL VOC consists of 1,464 train and 1,449 validation images. We use the high-quality pixel-level annotations of Cityscapes, comprising of 2975 train and 500 validation images. We evaluated all models on original image dimensions. ADE20K consists of 20,210 train, 2000 validation images, and 150 semantic classes.

Evaluation metrics. We apply mean Intersection-over-Union as performance metric (mIoU) for every model and average over severity levels. In addition, we use, and slightly modify, the concept of Corruption Error and relative Corruption Error from [39] as follows.

We use the term *Degradation D*, where $D = 1 - mIoU$ in place of *Error*. Degradations across severity levels,

Architecture	Blur						Noise					Digital				Weather				Geometric Distortion
	Clean	Motion	Defocus	Frosted Glass	Gaussian	PSF	Gaussian	Impulse	Shot	Speckle	Intensity	Brightness	Contrast	Saturate	JPEG	Snow	Spatter	Fog	Frost	
MobileNet-V2	72.0	53.5	49.0	45.3	49.1	70.5	6.4	7.0	6.6	16.6	26.9	51.7	46.7	32.4	27.2	13.7	38.9	47.4	17.3	65.5
ResNet-50	76.6	58.5	56.6	47.2	57.7	74.8	6.5	7.2	10.0	31.1	30.9	58.2	54.7	41.3	27.4	12.0	42.0	55.9	22.8	69.5
ResNet-101	77.1	59.1	56.3	47.7	57.3	75.2	13.2	13.9	16.3	36.9	39.9	59.2	54.5	41.5	37.4	11.9	47.8	55.1	22.7	69.7
Xception-41	77.8	61.6	54.9	51.0	54.7	76.1	17.0	17.3	21.6	43.7	48.6	63.6	56.9	51.7	38.5	18.2	46.6	57.6	20.6	73.0
Xception-65	78.4	63.9	59.1	52.8	59.2	76.8	15.0	10.6	19.8	42.4	46.5	65.9	59.1	46.1	31.4	19.3	50.7	63.6	23.8	72.7
Xception-71	78.6	64.1	60.9	52.0	60.4	76.4	14.9	10.8	19.4	41.2	50.2	68.0	58.7	47.1	40.2	18.8	50.4	64.1	20.2	71.0
ICNet	65.9	45.8	44.6	47.4	44.7	65.2	8.4	8.4	10.6	27.9	29.7	41.0	33.1	27.5	34.0	6.3	30.5	27.3	11.0	35.7
FCN8s-VGG16	66.7	42.7	31.1	37.0	34.1	61.4	6.7	5.7	7.8	24.9	18.8	53.3	39.0	36.0	21.2	11.3	31.6	37.6	19.7	36.9
DilatedNet	68.6	44.4	36.3	32.5	38.4	61.1	15.6	14.0	18.4	32.7	35.4	52.7	32.6	38.1	29.1	12.5	32.3	34.7	19.2	38.9
ResNet-38	77.5	54.6	45.1	43.3	47.2	74.9	13.7	16.0	18.2	38.3	35.9	60.0	50.6	46.9	14.7	13.5	45.9	52.9	22.2	43.2
PSPNet	78.8	59.8	53.2	44.4	53.9	76.9	11.0	15.4	15.4	34.2	32.4	60.4	51.8	30.6	21.4	8.4	42.7	34.4	16.2	43.4
GSCNN	80.9	58.9	58.4	41.9	60.1	80.3	5.5	2.6	6.8	24.7	29.7	75.9	61.9	70.7	12.0	12.4	47.3	67.9	32.6	42.7

Table 1: Average mIoU for clean and corrupted variants of the Cityscapes validation set for several network backbones of the DeepLabv3+ architecture (*top*) and non-DeepLab based models (*bottom*). Every mIoU is averaged over all available severity levels, except for corruptions of category noise where only the first three (of five) severity levels are considered. Xception based network backbones are usually most robust against each corruption. Most models are robust against our realistic PSF blur. Highest mIoU per corruption is bold.

which are defined by the ImageNet-C corruptions [39], are often aggregated. To make models mutually comparable, we divide the degradation D of a trained model f through the degradation of a reference model ref . With this, the *Corruption Degradation* (CD) of a trained model is defined as

$$CD_c^f = \left(\sum_{s=1}^5 D_{s,c}^f \right) / \left(\sum_{s=1}^5 D_{s,c}^{ref} \right) \quad (1)$$

where c denotes the corruption type (*e.g.*, Gaussian blur) and s its severity level. Please note that for *category noise*, only the first three severity levels are taken into account. While we predominately use CD for comparing the robustness of model architectures, we also consider the degradation of models relative to clean data, measured by the *relative Corruption Degradation* (rCD). We highlight the difference between CD and rCD in more detail in the supplement.

$$rCD_c^f = \left(\sum_{s=1}^5 D_{s,c}^f - D_{clean}^f \right) / \left(\sum_{s=1}^5 D_{s,c}^{ref} - D_{clean}^{ref} \right) \quad (2)$$

5.2. Benchmarking Network Backbones

We trained various network backbones (MobileNet-V2, ResNets, Xceptions) on the original, clean training-sets of PASCAL VOC 2012, the Cityscapes dataset, and ADE20K. Table 1 shows the average mIoU for the Cityscapes dataset, and each corruption type averaged over all severity levels. We refer to the supplement for the respective results for other datasets and individual severity levels.

As expected, for DeepLabv3+, Xception-71 exhibits the best performance for clean data with an mIoU of 78.6%¹. The bottom part of Table 1 shows the benchmark results of non-DeepLab based models.

Network backbone performance. Most Xception based models perform significantly better than ResNets and MobileNet-V2. GSCNN is the best performing architecture

on clean data of this benchmark.

Performance w.r.t. blur. Interestingly, all models (except DilatedNet and VGG16) handle PSF blur well, as the respective mIoU decreases only by roughly 2%. Thus, even a lightweight network backbone such as MobileNet-V2 is hardly vulnerable against this realistic type of blur. The number of both false positive and false negative pixel-level classifications increases, especially for far-distant objects. With respect to Cityscapes this means that persons are simply overlooked or confused with similar classes, such as rider. Please find some result images in the supplement.

Performance w.r.t. noise. Noise has a substantial impact on model performance. Hence we only averaged over the first three severity levels. Xception-based network backbones of DeepLabv3+ often perform similar or better than non-DeepLabv3+ models. MobileNet-V2, ICNet, VGG-16, and GSCNN handle the severe impact of image noise significantly worse than the other models.

Performance w.r.t. digital. The first severity levels of corruption types contrast, brightness, and saturation are handled well. However, JPEG compression decreases performance by a large margin. Notably, PSPNet and GSCNN have for this corruption halved or less mIoU than Xception-41 and -71, though their mIoU on clean data is similar.

Performance w.r.t. weather. Texture-corrupting distortions as snow and frost degrade mIoU of each model significantly.

Performance w.r.t. Geometric distortion. Models of DeepLabv3+ handle geometric distortion significantly better than non-DeepLabv3+ based models.

This benchmark indicates, in general, a similar result as in [26], that is image distortions corrupting the texture of an image (*e.g.*, image noise, snow, frost, JPEG), often have distinct negative effect on model performance compared to image corruptions preserving texture to a certain point (*e.g.*, blur, brightness, contrast, geometric distortion). To evaluate the robustness w.r.t. image corruptions of proposed network backbones, it is also interesting to consider Corruption Degradation (CD) and relative Corruption Degradation (rCD). Fig. 4 illustrates the mean CD and rCD with re-

¹Note that we were not able to reproduce the results from [14]. We conjecture that this is due to hardware limitations, as we could not set the suggested crop-size of 769×769 for Cityscapes.

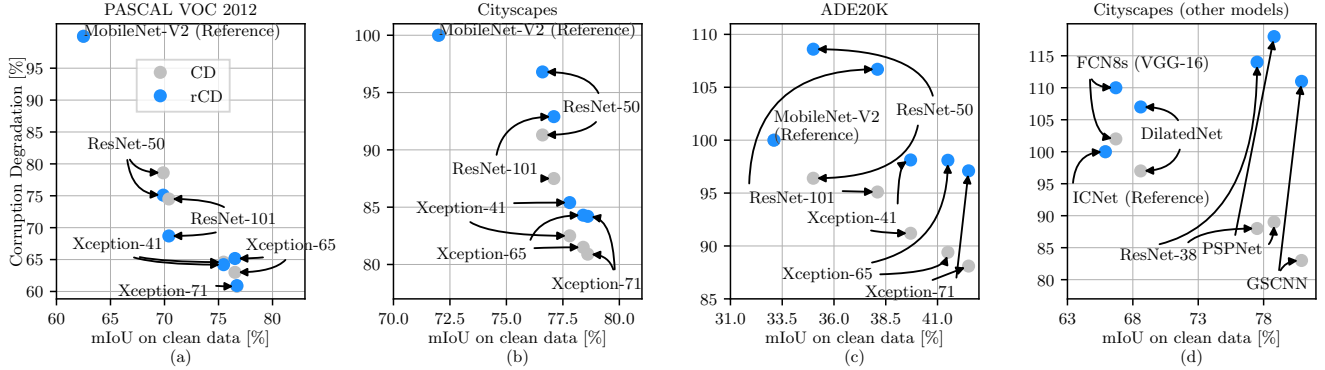


Figure 4: (a–c) CD and rCD for several network backbones of the DeepLabv3+ architecture evaluated on PASCAL VOC 2012, the Cityscapes dataset, and ADE20K. MobileNet-V2 is the reference model in each case. rCD and CD values below 100 % represent higher robustness than the reference model. In almost every case, model robustness increases with model performance (*i.e.* mIoU on clean data). Xception-71 is the most robust network backbone on each dataset. (d) CD and rCD for non-DeepLabv3+ based models evaluated on Cityscapes. While CD decreases with increasing performance on clean data, rCD is larger than 100 %.

spect to the mIoU for *clean* images (lower values correspond to higher robustness regarding the reference model). Each dot depicts the performance of one network backbone, averaged over all corruptions except for PSF blur². Subplot a–c illustrates respective results for PASCAL VOC 2012, Cityscapes, and ADE20K. On each dataset, Xception-71 is the most robust network backbone for DeepLabv3+ architecture. Interestingly, rCD decreases often with increasing model performance, except for Xception-65 on PASCAL VOC 2012 (Fig. 4 a) and ResNets on ADE20K (Fig. 4 c). The latter result indicates that ResNet-based backbones are vulnerable when applied for a large-scale dataset as ADE20K. Fig. 4 d presents the respective result for several non-DeepLabv3+ based segmentation models. The rCD for these models increases slightly. On the other hand, CD decreases mostly with increasing model performance on clean data. The authors of [39] report the same result for the task of full-image classification: The rCD for established networks stays relatively constant, even though model performance on clean data differs significantly, as Fig. 4 d indicate. When we, however, evaluate within a semantic segmentation architecture, as DeepLabv3+, the contrary result (*i.e.*, decreasing rCD) is generally observed. The following speculation may also give further insights. Geirhos *et al.* [26] stated recently that (i) DCNNs for full-image classification examine local textures, rather than global shapes of an object, to solve the task at hand, and (ii) model performance w.r.t. image corruption increases when the model relies more on object shape (rather than object texture). Transferring these results to the task of semantic segmentation, Xception-based backbones might have a more pronounced shape bias than others (*e.g.*, ResNets), resulting hence in a higher rCD score w.r.t. image corruption. This

may be an interesting topic for future work, however, beyond the scope of this paper.

5.3. Ablation Study on Cityscapes

Instead of solely comparing robustness across network backbones, we now conduct an extensive ablation study for DeepLabv3+. We employ the state-of-the-art performing Xception-71 (XC-71), Xception-65 (XC-65), Xception-41 (XC-41), ResNet-101, ResNet-50 and, their lightweight counterpart, MobileNet-V2 (MN-V2) (width multiplier 1, 224×224), as network backbones. XC-71 is the best performing backbone on clean data, but at the same time, computationally most expensive. The efficient MN-V2, on the other hand, requires roughly ten times less storage space. We ablated for each network backbone of the DeepLabv3+ architecture the same architectural properties as listed in section 4.2. Each ablated variant has been re-trained on clean data of Cityscapes, PASCAL VOC 2012, and ADE20K, summing up to over 100 trainings. Table 2 shows the averaged mIoU for XC-71, evaluated on Cityscapes. We refer to the supplement for the results of the remaining backbones. In the following sections, we discuss the most distinct, statistically significant results.

We see that with Dense Prediction Cell (DPC), we achieve the highest mIoU on clean data followed by the reference model. We also see that removing ASPP reduces mIoU significantly.

To better understand the robustness of each ablated model, we illustrate the average CD within corruption categories (*e.g.*, blur) in Fig. 5 (bars above 100 % indicate reduced robustness compared to the respective reference model).

Effect of ASPP. Removal of ASPP reduces model performance significantly (Table 2 first column). We refer to the supplement for an evaluation.

Effect of AC. Atrous convolutions (AC) generally show a positive effect w.r.t. corruptions of type blur for most net-

²Due to the considerably smaller impact of PSF blur on model performance, small changes in mIoU of only tenths percentage can have a significant impact on the corresponding rCD.

DeepLabv3+ Backbone	Blur						Noise					Digital				Weather				
	Clean	Motion	Defocus	Frosted Glass	Gaussian	PSF	Gaussian	Impulse	Shot	Speckle	Intensity	Brightness	Contrast	Saturate	JPEG	Snow	Spatter	Fog	Frost	Geometric Distortion
Xception-71	78.6	64.1	60.9	52.0	60.4	76.4	14.9	10.8	19.4	41.2	50.2	68.0	58.7	47.1	40.2	18.8	50.4	64.1	20.2	71.0
w/o ASPP	73.9	60.7	59.5	51.5	58.4	72.8	18.5	14.7	22.3	39.8	44.7	63.4	56.2	42.7	39.9	17.6	49.0	58.3	21.8	69.3
w/o AC	77.9	62.2	57.9	51.8	58.2	76.1	7.7	5.7	11.2	32.8	43.2	67.6	55.6	46.0	40.7	18.2	50.1	61.1	21.6	71.1
w/o ASPP+w/ DPC	78.8	62.8	59.4	52.6	58.2	76.9	7.3	2.8	10.7	33.0	42.4	64.8	59.4	45.3	32.0	14.4	48.6	64.0	20.8	72.1
w/o LRL	77.9	64.2	63.2	50.7	62.2	76.7	13.9	9.3	18.2	41.3	49.9	64.5	59.2	44.3	36.1	16.9	48.7	64.3	21.3	71.3
w/ GAP	78.6	64.2	61.7	55.9	60.7	77.8	9.7	8.4	13.9	36.9	45.6	68.0	60.2	48.4	40.6	16.8	51.0	62.1	20.9	73.6

Table 2: Average mIoU for clean and corrupted variants of the Cityscapes validation dataset for Xception-71 and five corresponding architectural ablations. Based on DeepLabv3+ we evaluate the removal of atrous spatial pyramid pooling (ASPP), atrous convolutions (AC), and long-range link (LRL). We further replaced ASPP by Dense Prediction Cell (DPC) and utilized global average pooling (GAP). Mean-IoU is averaged over severity levels. The standard deviation for image noise is 0.2 or less. Highest mIoU per corruption is bold.

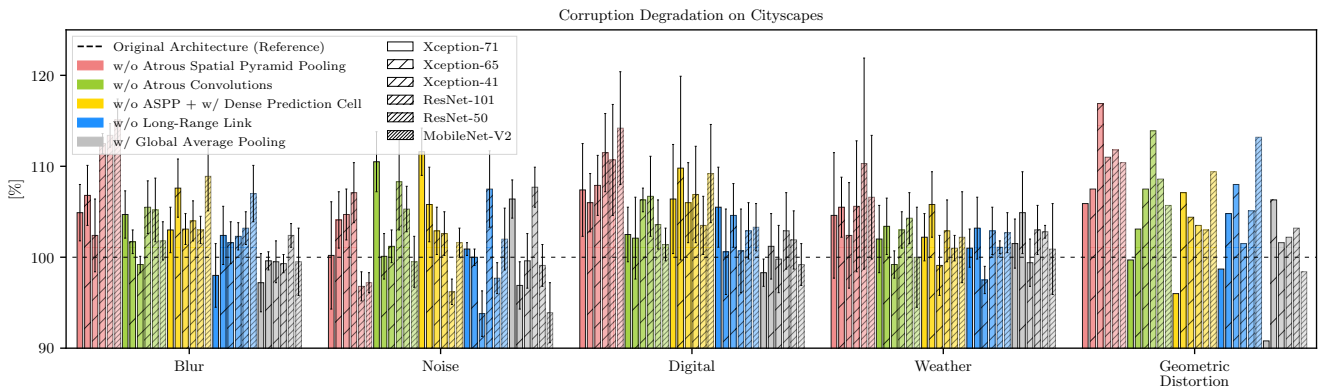


Figure 5: CD evaluated on Cityscapes for the proposed ablated variants of the DeepLabv3+ architecture w.r.t. image corruptions, employing six different network backbones. Bars above 100% represent a decrease in performance compared to the respective reference architecture. Each ablated architecture is re-trained on the original training dataset. Removing ASPP reduces the model performance significantly. Atrous convolutions increase robustness against blur. The model becomes vulnerable against most effects when Dense Prediction Cell is used. Each bar is the average CD of a corruption category, except for geometric distortion (error bars indicate the standard deviation).

work backbones, especially for XC-71 and ResNets. For example, without AC, the average mIoU for defocus blur decreases by 3.8% for ResNet-101 (CD = 109%). Blur reduces high-frequency information of an image, leading to similar signals stored in consecutive pixels. Applying AC can hence increase the amount of information per convolution filter, by skipping direct neighbors with similar signals. Regarding XC-71 and ResNets, AC clearly enhance robustness on noise-based corruptions. The mIoU for the first severity level of Gaussian noise are 12.2% (XC-71), 10.8% (ResNet-101), 8.0% (ResNet-50) less than respective reference. AC generally exhibit also a positive effect w.r.t. geometric distortion. For MN-V2 and ResNets, the averaged mIoU reduces by up to 4.2% ($CD^{ResNet-50} = 109\%$, $CD^{ResNet-101} = 114\%$, $CD^{MN-V2} = 106\%$). In summary, AC often increase robustness against a broad range of network backbones and image corruptions.

Effect of DPC. When employing Dense Prediction Cell (DPC) instead of ASPP, the models become clearly vulnerable against corruptions of most categories. While this ablated architecture reaches the highest mIoU on clean data for XC-71, it is less robust to a broad range of corruptions. For example, CD for defocus blur on MN-V2 and XC-65 are 113% and 110%, respectively. Average mIoU decreases by 6.8% and by 4.1%. For XC-71, CD for all corruptions of category noise are within 109% and 115%.

The average mIoU of this ablated variant is least for all, but one type of noise (Table 2). Similar behavior can be observed for other corruptions and backbones. DPC has been found through a neural-architecture-search (NAS, *e.g.*, [92, 91, 65]) with the objective of maximizing performance on clean data. This result indicates that such architectures tend to over-fit on this objective, *i.e.* clean data. It may be an interesting topic to evaluate robustness w.r.t. image corruptions for other NAS-based architectures as future work, however, is beyond the scope of this paper. Consequently, performing NAS on corrupted data might deliver interesting findings of robust architectural properties—similar as in [19] w.r.t. adversarial examples. We further hypothesize that DPC learns less multi-scale representations than ASPP, which may be useful against common corruptions. We discuss this hypothesis in the supplement.

Effect of LRL. A long-range link (LRL) appears to be very beneficial for ResNet-101 against image noise. The model struggles especially for our noise model, as its CD equals 116%. For XC-71, corruptions of category digital as *brightness* have considerably high CDs (*e.g.*, $CD^{XC-71} = 111\%$). For MN-V2, removing LRL decreases robustness w.r.t. defocus blur and geometric distortion as average mIoU reduces by 5.1% (CD = 110%) and 4.6% (CD = 113%).

Effect of GAP. Global average pooling (GAP) increases

Ablation	w/o ASPP						w/o AC						w/o ASPP w/ DPC						w/o LRL						w/ GAP					
Network Backbone	ResNet– 50 101		Xception– 41 65 71				ResNet– 50 101		Xception– 41 65 71				ResNet– 50 101		Xception– 41 65 71				ResNet– 50 101		Xception– 41 65 71				ResNet– 50 101		Xception– 41 65 71			
Blur	120	117	115	118	119		102	99	99	98	100		103	101	100	104	109	102	101	97	102	104		98	98	98	95	101		
Noise	124	127	122	126	123		100	106	103	100	101		99	102	98	103	105	100	103	96	101	95		94	97	99	97	98		
Digital	133	128	127	124	124		103	101	102	101	103		104	102	101	103	105	103	102	98	103	103		95	96	98	97	94		
Weather	121	119	120	114	118		101	100	101	99	104		102	100	103	102	105	101	100	100	101	103		94	93	98	95	96		
Geometric Distortion	133	124	128	118	117		104	102	104	100	102		107	106	104	100	101	105	105	100	102	102		99	98	102	101	101		

Table 3: CD evaluated on PASCAL VOC 2012 for ablated network backbones of the DeepLabv3+ architecture w.r.t. image corruptions.

slightly robustness w.r.t. blur for most Xceptions. Interestingly, when applied in XC-71 (ResNet-101), the model is vulnerable to image noise. Corresponding CD values range between 103 % and 109 % (106 % and 112 %).

5.4. Ablation Study on Pascal VOC 2012

We generally observe that the effect of the architectural ablations for DeepLabv3+ trained on PASCAL VOC 2012 is not always similar to previous results on Cityscapes (see Table 3). Since this dataset is less complex than Cityscapes, the mIoU of ablated architectures differ less.

We do not evaluate results on MN-V2, as the model is not capable of giving a comparable performance. Please see the supplement corresponding mIoU scores.

Effect of ASPP. Similar to the results on Cityscapes, removal of ASPP reduces model performance of each network backbone significantly.

Effect of AC. Unlike on Cityscapes, atrous convolutions show no positive effect against blur. We explain this with the fundamentally different datasets. On Cityscapes, a model without AC often overlooks classes covering small image-regions, especially when far away. Such images are hardly present in PASCAL VOC 2012. As on Cityscapes, AC slightly helps performance for most models w.r.t. geometric distortion. For XC-41 and ResNet-101, we see a positive effect of AC against image noise.

Effect of DPC. As on Cityscapes, DPC decreases robustness for many corruptions. Generally, CD increases from XC-41 to XC-71. The impact on XC-71 is especially strong as indicated by the CD score, averaged over all corruptions, is 106 %. A possible explanation might be that the neural-architecture-search (NAS) *e.g.*, [92, 91, 65] has been performed on XC-71 and enhances, therefore, the over-fitting effect additionally, as discussed in section 5.3.

Effect of LRL. Removing LRL increases robustness against noise for XC-71 and XC-41, probably due to discarding early features (we refer to the supplement for discussion). However, this finding does not hold for XC-65. As reported in section 5.2, on PASCAL VOC 2012, XC-65 is also the most robust model against noise. Regarding ResNets, the LRL affects the image corruption of category geometric distortion the most.

Effect of GAP. When global average pooling is applied,

the overall robustness of every network backbone increases particularly significant. The mIoU on clean data increases for every model (up to 2.2 % for ResNet-101, probably due to the difference between PASCAL VOC 2012 and the remaining dataset (we refer to supplement).

5.5. Ablation Study on ADE20K

The performance on clean data ranges from MN-V2 (mIoU of 33.1 %) to XC-71 using DPC, as best-performing model, achieving an mIoU of 42.5 % (detailed results listed in the supplement). The performance on clean data for most Xception-based backbones (ResNets) is highest when Dense Prediction Cell (global average pooling) is used. Our evaluation shows that the mean CD for each ablated architecture is often close to 100.0 %. The impact of proposed architectural properties on model performance is thus on the large-scale dataset ADE20K hardly present. A possible explanation is probably that the effect of architectural design choices becomes more decisive, and respective impacts are more pronounced when models perform well, *i.e.* have large mIoU. DeepLabv3+ performs much poorer on ADE20K than, *e.g.*, on the Cityscapes dataset.

The tendencies of the previous findings are nevertheless present. Regarding XC-71, for example, the corresponding means of both CD and rCD for DPC are respectively 101 % and 107 %, showing its robustness is again less than the reference model. ASPP, on the other hand, affects segmentation performance also significantly.

6. Conclusion

We have presented a detailed, large-scale evaluation of state-of-the-art semantic segmentation models with respect to real-world image corruptions. Based on the study, we can introduce robust model design rules: Atrous convolutions are generally recommended since they increase robustness against many corruptions. The vulnerability of Dense Prediction Cell to many corruptions must be considered, especially in low-light and safety-critical applications. The ASPP module is important for decent model performance, especially for digitally and geometrically distorted input. Global average pooling should always be used on PASCAL VOC 2012. Our detailed study may help to improve on the state-of-the-art for robust semantic segmentation models.

References

- [1] Martin Abadi, Paul Barham, Jianmin Chen, Zhifeng Chen, Andy Davis, Jeffrey Dean, Matthieu Devin, Sanjay Ghemawat, Geoffrey Irving, Michael Isard, Manjunath Kudlur, Josh Levenberg, Rajat Monga, Sherry Moore, Derek G. Murray, Benoit Steiner, Paul Tucker, Vijay Vasudevan, Pete Warden, Martin Wicke, Yuan Yu, and Xiaoqiang Zheng. TensorFlow: A system for large-scale machine learning. In *12th USENIX Symposium on Operating Systems Design and Implementation (OSDI 16)*, pages 265–283, 2016.
- [2] Anurag Arnab, Ondrej Miksik, and Philip H. S. Torr. On the Robustness of Semantic Segmentation Models to Adversarial Attacks. In *CVPR*, 2018.
- [3] Aharon Azulay and Yair Weiss. Why do deep convolutional networks generalize so poorly to small image transformations? *CoRR*, abs/1805.12177, 2018.
- [4] Vijay Badrinarayanan, Alex Kendall, and Roberto Cipolla. SegNet: A Deep Convolutional Encoder-Decoder Architecture for Image Segmentation. In *PAMI*, 2017.
- [5] Chris H Bahnsen, David Vzquez, Antonio M Lpez, and Thomas B Moeslund. Learning to Remove Rain in Traffic Surveillance by Using Synthetic Data. In *VISI-GRAPP*, 2019.
- [6] Akhilan Boopathy, Tsui-Wei Weng, Pin-Yu Chen, Sijia Liu, and Luca Daniel. CNN-Cert: An Efficient Framework for Certifying Robustness of Convolutional Neural Networks. In *AAAI*, Jan. 2019.
- [7] Tejas S. Borkar and Lina J. Karam. DeepCorrect: Correcting DNN models against Image Distortions. *arXiv:1705.02406 [cs.CV]*, 2017.
- [8] Nicholas Carlini and David Wagner. Adversarial Examples Are Not Easily Detected: Bypassing Ten Detection Methods. In *Proceedings of the 10th ACM Workshop on Artificial Intelligence and Security, AISec '17*, pages 3–14, New York, NY, USA, 2017. ACM.
- [9] Nicholas Carlini and David A. Wagner. Towards Evaluating the Robustness of Neural Networks. *2017 IEEE Symposium on Security and Privacy (SP)*, 2017.
- [10] Liang-Chieh Chen, Maxwell D. Collins, Yukun Zhu, George Papandreou, Barret Zoph, Florian Schroff, Hartwig Adam, and Jonathon Shlens. Searching for Efficient Multi-Scale Architectures for Dense Image Prediction. In *NIPS*, 2018.
- [11] Liang-Chieh Chen, George Papandreou, Iasonas Kokkinos, Kevin Murphy, and Alan L. Yuille. Semantic Image Segmentation with Deep Convolutional Nets and Fully Connected CRFs. In *ICLR*, volume abs/1412.7062, 2015.
- [12] Liang-Chieh Chen, George Papandreou, Iasonas Kokkinos, Kevin Murphy, and Alan L. Yuille. DeepLab: Semantic Image Segmentation with Deep Convolutional Nets, Atrous Convolution, and Fully Connected CRFs. In *TPAMI*, 2017.
- [13] Liang-Chieh Chen, George Papandreou, Florian Schroff, and Hartwig Adam. Rethinking Atrous Convolution for Semantic Image Segmentation, 2017.
- [14] Liang-Chieh Chen, Yukun Zhu, George Papandreou, Florian Schroff, and Hartwig Adam. Encoder-Decoder with Atrous Separable Convolution for Semantic Image Segmentation. In *ECCV*, 2018.
- [15] Yuhua Chen, Wen Li, Christos Sakaridis, Dengxin Dai, and Luc Van Gool. Domain adaptive faster r-cnn for object detection in the wild. In *CVPR*, pages 3339–3348, 2018.
- [16] Francois Chollet. Xception: Deep Learning with Depthwise Separable Convolutions. In *CVPR*, 2017.
- [17] Moustapha Cisse, Piotr Bojanowski, Edouard Grave, Yann Dauphin, and Nicolas Usunier. Parseval Networks: Improving Robustness to Adversarial Examples. In Doina Precup and Yee Whye Teh, editors, *Proceedings of the 34th International Conference on Machine Learning*, Proceedings of Machine Learning Research, International Convention Centre, Sydney, Australia, 2017. PMLR.
- [18] Marius Cordts, Mohamed Omran, Sebastian Ramos, Timo Rehfeld, Markus Enzweiler, Rodrigo Benenson, Uwe Franke, Stefan Roth, and Bernt Schiele. The Cityscapes Dataset for Semantic Urban Scene Understanding. In *CVPR*, 2016.
- [19] Ekin Dogus Cubuk, Barret Zoph, Samuel Stern Schoenholz, and Quoc V. Le. *Intriguing Properties of Adversarial Examples*. 2018.
- [20] Dengxin Dai and Luc Van Gool. Dark model adaptation: Semantic image segmentation from daytime to nighttime. In *ITSC*, pages 3819–3824. IEEE, 2018.
- [21] J. Deng, W. Dong, R. Socher, L.-J. Li, K. Li, and L. Fei-Fei. ImageNet: A Large-Scale Hierarchical Image Database. In *CVPR*, 2009.
- [22] Samuel Dodge and Lina Karam. A study and comparison of human and deep learning recognition performance under visual distortions. In *2017 26th international conference on computer communication and networks (ICCCN)*, pages 1–7. IEEE, 2017.
- [23] Samuel F. Dodge and Lina J. Karam. Understanding how image quality affects deep neural networks. In *Quomex*, 2016.
- [24] Mark Everingham, Luc Van Gool, Christopher K. I. Williams, John Winn, and Andrew Zisserman. The Pascal Visual Object Classes (VOC) Challenge. In *IJCV*, 2010.
- [25] A. W. Fitzgibbon. Simultaneous linear estimation of multiple view geometry and lens distortion. In *CVPR*, volume 1, pages I–I, Dec. 2001.
- [26] R. Geirhos, P. Rubisch, C. Michaelis, M. Bethge, F. A. Wichmann, and W. Brendel. ImageNet-trained CNNs are biased towards texture; increasing shape bias improves accuracy and robustness. In *ICLR*, May 2019.
- [27] Robert Geirhos, Carlos R. Medina Temme, Jonas Rauber, Heiko H. Schtt, Matthias Bethge, and Felix A. Wichmann. Generalisation in humans and deep neural networks. *NIPS*, abs/1808.08750, 2018.
- [28] Justin Gilmer, Nicolas Ford, Nicholas Carlini, and Ekin Cubuk. Adversarial Examples Are a Natural Consequence of Test Error in Noise. In Kamalika Chaudhuri and Ruslan Salakhutdinov, editors, *Proceedings of the 36th International Conference on Machine Learning*, volume 97 of *Proceedings of Machine Learning Research*, pages 2280–2289, Long Beach, California, USA, June 2019. PMLR.
- [29] Ian Goodfellow, Yoshua Bengio, and Aaron Courville. *Deep Learning*. MIT Press, 2016.

- [30] K. Grauman and T. Darrell. The Pyramid Match Kernel: Discriminative Classification with Sets of Image Features. In *ICCV*, 2005.
- [31] Shixiang Gu and Luca Rigazio. Towards Deep Neural Network Architectures Robust to Adversarial Examples. *NIPS Workshop on Deep Learning and Representation Learning*, abs/1412.5068, 2014.
- [32] Bharath Hariharan, Pablo Arbeliz, Ross Girshick, and Jitendra Malik. Hypercolumns for object segmentation and fine-grained localization. In *CVPR*, pages 447–456, 2015.
- [33] Richard Hartley and Andrew Zisserman. *Multiple view geometry in computer vision*. Cambridge university press, 2003.
- [34] S. Hasirlioglu, A. Kamann, I. Doric, and T. Brandmeier. Test methodology for rain influence on automotive surround sensors. In *ITSC*, pages 2242–2247, Nov. 2016.
- [35] Kaiming He, Xiangyu Zhang, Shaoqing Ren, and Jian Sun. Spatial Pyramid Pooling in Deep Convolutional Networks for Visual Recognition. In *ECCV*, 2014.
- [36] Kaiming He, Xiangyu Zhang, Shaoqing Ren, and Jian Sun. Delving Deep into Rectifiers: Surpassing Human-Level Performance on ImageNet Classification. *ICCV*, pages 1026–1034, 2015.
- [37] Kaiming He, Xiangyu Zhang, Shaoqing Ren, and Jian Sun. Deep Residual Learning for Image Recognition. In *CVPR*, 2016.
- [38] Glenn E Healey and Raghava Kondepudy. Radiometric CCD camera calibration and noise estimation. *PAMI*, 16(3):267–276, 1994.
- [39] Dan Hendrycks and Thomas Dietterich. Benchmarking Neural Network Robustness to Common Corruptions and Perturbations. *Proceedings of the International Conference on Learning Representations*, 2019.
- [40] Joo F. Henriques and Andrea Vedaldi. Warped Convolutions: Efficient Invariance to Spatial Transformations. In *ICML*, 2017.
- [41] M. Holschneider, R. Kronland-Martinet, J. Morlet, and P. Tchamitchian. A Real-Time Algorithm for Signal Analysis with the Help of the Wavelet Transform. In J.-M. Combes, A. Grossmann, and P. Tchamitchian, editors, *Wavelets. Time-Frequency Methods and Phase Space*, page 286, 1989.
- [42] Andrew G. Howard, Menglong Zhu, Bo Chen, Dmitry Kalenichenko, Weijun Wang, Tobias Weyand, Marco Andreetto, and Hartwig Adam. MobileNets: Efficient Convolutional Neural Networks for Mobile Vision Applications. *CoRR*, abs/1704.04861, 2017.
- [43] Gao Huang, Zhuang Liu, Laurens van der Maaten, and Kilian Q. Weinberger. Densely Connected Convolutional Networks. *CVPR*, pages 2261–2269, 2017.
- [44] Xiaowei Huang, Marta Z. Kwiatkowska, Sen Wang, and Min Wu. Safety Verification of Deep Neural Networks. In *CAV*, 2017.
- [45] Ioffe, Sergey and Szegedy, Christian. Batch Normalization: Accelerating Deep Network Training by Reducing Internal Covariate Shift. In *ICML*, 2015.
- [46] Joel Janai, Fatma Gney, Aseem Behl, and Andreas Geiger. Computer Vision for Autonomous Vehicles: Problems, Datasets and State-of-the-Art. *Arxiv*, 2017.
- [47] N. Joshi, R. Szeliski, and D. J. Kriegman. PSF estimation using sharp edge prediction. In *CVPR*, pages 1–8, June 2008.
- [48] A. Kamann, S. Hasirlioglu, I. Doric, T. Speth, T. Brandmeier, and U. T. Schwarz. Test Methodology for Automotive Surround Sensors in Dynamic Driving Situations. In *2017 IEEE 85th Vehicular Technology Conference (VTC Spring)*, pages 1–6, June 2017.
- [49] Tsung-Wei Ke, Michael Maire, and Stella X. Yu. Multigrid Neural Architectures. In *CVPR*, pages 4067–4075, 2017.
- [50] Alex Krizhevsky, Ilya Sutskever, and Geoffrey E Hinton. Imagenet classification with deep convolutional neural networks. In *Advances in neural information processing systems*, pages 1097–1105, 2012.
- [51] Svetlana Lazebnik, Cordelia Schmid, and Jean Ponce. Beyond Bags of Features: Spatial Pyramid Matching for Recognizing Natural Scene Categories. In *CVPR*, Washington, DC, USA, 2006.
- [52] Yann LeCun, Yoshua Bengio, and Geoffrey E. Hinton. Deep learning. In *Nature*, 2015.
- [53] Yann Lecun, Lon Bottou, Yoshua Bengio, and Patrick Haffner. Gradient-based learning applied to document recognition. *Proceedings of the IEEE*, 1998.
- [54] Min Lin, Qiang Chen, and Shuicheng Yan. Network in network. In *ICLR*, 2014.
- [55] C. Liu, R. Szeliski, S. Bing Kang, C. L. Zitnick, and W. T. Freeman. Automatic Estimation and Removal of Noise from a Single Image. *PAMI*, 30(2):299–314, Feb. 2008.
- [56] Jonathan Long, Evan Shelhamer, and Trevor Darrell. Fully Convolutional Networks for Semantic Segmentation. In *CVPR*, volume abs/1411.4038, 2015.
- [57] J. Lukas, J. Fridrich, and M. Goljan. Digital camera identification from sensor pattern noise. *IEEE Transactions on Information Forensics and Security*, 1(2):205–214, June 2006.
- [58] Jan Hendrik Metzen, Tim Genewein, Volker Fischer, and Bastian Bischoff. On Detecting Adversarial Perturbations. In *ICLR*, 2017.
- [59] C. Michaelis, B. Mitzkus, R. Geirhos, E. Rusak, O. Bringmann, A. S. Ecker, M. Bethge, and W. Brendel. Benchmarking Robustness in Object Detection: Autonomous Driving when Winter is Coming. In *Machine Learning for Autonomous Driving Workshop, NeurIPS 2019*, volume 190707484, July 2019.
- [60] Jashojit Mukherjee, K Praveen, and Venugopala Madambu. Visual Quality Enhancement Of Images Under Adverse Weather Conditions. In *ITSC*, pages 3059–3066. IEEE, 2018.
- [61] Behnam Neyshabur, Srinadh Bhojanapalli, David McAllester, and Nathan Srebro. Exploring Generalization in Deep Learning. In *NIPS*, 2017.
- [62] George Papandreou, Iasonas Kokkinos, and Pierre-Andr Savalle. Modeling local and global deformations in Deep Learning: Epitomic convolution, Multiple Instance Learning, and sliding window detection. In *CVPR*, pages 390–399, 2015.
- [63] Adam Paszke, Abhishek Chaurasia, Sangpil Kim, and Eugenio Culurciello. ENet: A Deep Neural Network Architecture for Real-Time Semantic Segmentation. *CoRR*, abs/1606.02147, 2016.

- [64] Adam Paszke, Sam Gross, Soumith Chintala, Gregory Chanan, Edward Yang, Zachary DeVito, Zeming Lin, Alban Desmaison, Luca Antiga, and Adam Lerer. Automatic Differentiation in PyTorch. In *NIPS Autodiff Workshop*, 2017.
- [65] Hieu Pham, Melody Y Guan, Barret Zoph, Quoc V Le, and Jeff Dean. Efficient neural architecture search via parameter sharing. *ICML*, 2018.
- [66] Haozhi Qi, Zheng Zhang, Bin Xiao, Han Hu, Bowen Cheng, Yichen Wei, and Jifeng Dai. Deformable convolutional networks coco detection and segmentation challenge 2017 entry. In *ICCV COCO Challenge Workshop*, volume 15, 2017.
- [67] Joseph Redmon, Santosh Kumar Divvala, Ross B. Girshick, and Ali Farhadi. You Only Look Once: Unified, Real-Time Object Detection. In *CVPR*, pages 779–788, 2016.
- [68] Christos Sakaridis, Dengxin Dai, and Luc Van Gool. Semantic foggy scene understanding with synthetic data. *IJCV*, 126(9):973–992, 2018.
- [69] Christos Sakaridis, Dengxin Dai, and Luc Van Gool. Guided Curriculum Model Adaptation and Uncertainty-Aware Evaluation for Semantic Nighttime Image Segmentation. In *ICCV*, 2019.
- [70] Mark Sandler, Andrew Howard, Menglong Zhu, Andrey Zhmoginov, and Liang-Chieh Chen. MobileNetV2: Inverted Residuals and Linear Bottlenecks. In *CVPR*, 2018.
- [71] Pierre Sermanet, David Eigen, Xiang Zhang, Michal Mathieu, Robert Fergus, and Yann Lecun. Overfeat: Integrated recognition, localization and detection using convolutional networks. In *ICLR*, 2014.
- [72] Meet P. Shah. Semantic Segmentation Architectures Implemented in PyTorch. <https://github.com/meetshah1995/pytorch-semseg>, 2017.
- [73] Shishir Shah and JK Aggarwal. Intrinsic parameter calibration procedure for a (high-distortion) fish-eye lens camera with distortion model and accuracy estimation. *Pattern Recognition*, 29(11):1775–1788, 1996.
- [74] Karen Simonyan and Andrew Zisserman. Very Deep Convolutional Networks for Large-Scale Image Recognition. In *ICLR*, 2015.
- [75] Zhun Sun, Mete Ozay, Yan Zhang, Xing Liu, and Takayuki Okatani. Feature Quantization for Defending Against Distortion of Images. In *CVPR*, June 2018.
- [76] Christian Szegedy, Wei Liu, Yangqing Jia, Pierre Sermanet, Scott Reed, Dragomir Anguelov, Dumitru Erhan, Vincent Vanhoucke, and Andrew Rabinovich. Going deeper with convolutions. In *CVPR*, 2015.
- [77] Towaki Takikawa, David Acuna, Varun Jampani, and Sanja Fidler. Gated-SCNN: Gated Shape CNNs for Semantic Segmentation. *ICCV*, 2019.
- [78] Igor Vasiljevic, Ayan Chakrabarti, and Gregory Shakhnarovich. Examining the Impact of Blur on Recognition by Convolutional Networks. *arXiv:1611.05760 [cs.CV]*, abs/1611.05760, 2016.
- [79] Georg Volk, Mueller Stefan, Alexander von Bernuth, Dennis Hospach, and Oliver Bringmann. Towards Robust CNN-Based Object Detection through Augmentation with Synthetic Rain Variations. In *ITSC*, 2019.
- [80] Reg G Willson. Modeling and calibration of automated zoom lenses. In *Videometrics III*, volume 2350, pages 170–187. International Society for Optics and Photonics, 1994.
- [81] Zifeng Wu, Chunhua Shen, and Anton Van Den Hengel. Wider or deeper: Revisiting the resnet model for visual recognition. *Pattern Recognition*, 90:119–133, 2019.
- [82] Jonghwa Yim and Kyung-Ah Sohn. Enhancing the Performance of Convolutional Neural Networks on Quality Degraded Datasets. *DICTA*, 2017.
- [83] Ian T Young, Jan J Gerbrands, and Lucas J Van Vliet. *Fundamentals of image processing*, volume 841. Delft University of Technology Delft, 1998.
- [84] Fisher Yu and Vladlen Koltun. Multi-Scale Context Aggregation by Dilated Convolutions. In *ICLR*, 2016.
- [85] Hengshuang Zhao, Xiaojuan Qi, Xiaoyong Shen, Jianping Shi, and Jiaya Jia. ICNet for Real-Time Semantic Segmentation on High-Resolution Images. In *ECCV*, 2018.
- [86] Hengshuang Zhao, Jianping Shi, Xiaojuan Qi, Xiaogang Wang, and Jiaya Jia. Pyramid Scene Parsing Network. In *CVPR*, 2017.
- [87] Stephan Zheng, Yang Song, Thomas Leung, and Ian J. Goodfellow. Improving the Robustness of Deep Neural Networks via Stability Training. In *CVPR*, pages 4480–4488, 2016.
- [88] Bolei Zhou, Hang Zhao, Xavier Puig, Sanja Fidler, Adela Barriuso, and Antonio Torralba. Scene parsing through ade20k dataset. In *CVPR*, pages 633–641, 2017.
- [89] Bolei Zhou, Hang Zhao, Xavier Puig, Tete Xiao, Sanja Fidler, Adela Barriuso, and Antonio Torralba. Semantic understanding of scenes through the ade20k dataset. *IJCV*, pages 1–20, 2016.
- [90] Yiren Zhou, Sibo Song, and Ngai-Man Cheung. On Classification of Distorted Images with Deep Convolutional Neural Networks. *ICASSP*, 2017.
- [91] Barret Zoph and Quoc V. Le. Neural Architecture Search with Reinforcement Learning. 2017.
- [92] Barret Zoph, Vijay Vasudevan, Jonathon Shlens, and Quoc V Le. Learning transferable architectures for scalable image recognition. In *CVPR*, pages 8697–8710, 2018.

Supplemental Material

We provide further information about the utilized image corruptions and the conducted experiments. In more detail, we first show examples of every image corruption, and we give further details of our proposed image corruptions (section A). To make the image corruptions mutually comparable, we provide the Signal-to-Noise ratio for image corruptions of category noise (section A.3).

In section B, we provide supplementary information about the experimental setup (section B.1, B.2), we explain the difference of the utilized evaluation metrics (*i.e.*, CD and rCD) in more detail (section B.3), we discuss possible causes of the effect of architectural design choices (section B.4), and we show qualitative results (section B.5).

In addition, we report the individual evaluation metric scores (*i.e.*, mIoU, CD, and rCD) for Cityscapes (section B.6), PASCAL VOC 2012 (section B.7), and ADE20K (section B.8). We further show the performance of many models for different severity levels of many image corruptions (section B.10).

A. Image Corruption Models

A.1. ImageNet-C

In this section, we illustrate the used image corruptions of ImageNet-C³. Figure A.1 shows the image corruptions of the categories blur, noise, digital, and weather of ImageNet-C. To make the image corruption clearly visible, we selected each example of severity level three or higher. The Figure is best viewed in color.

A.2. Proposed Image Corruptions

In this section, we provide more details about our image corruptions, *i.e.*, the proposed image noise model, PSF blur, and geometric distortion. Figure A.3 shows examples of our proposed image corruptions.

Intensity-Dependent Noise Model. In the main paper, we proposed a noise model that incorporates intensity-dependent chrominance and luminance noise components that are both added to original pixel intensities in linear color space. Here, the term *chrominance noise* means that a random noise component for an image pixel is drawn for each color channel independently, resulting thus in color noise. *Luminance noise*, on the other hand, refers to a random noise value that is added to each channel of a pixel equally, resulting hence in gray-scale noise. We model the noisy pixel intensity for a color channel c as a random vari-

able $I_{noise,c}$:

$$I_{noise,c}(\Phi_c, N_{luminance}, N_{chrominance,c}; w_s) = \log_2(2^{\Phi_c} + w_s \cdot (N_{luminance} + N_{chrominance,c})) \quad (3)$$

where Φ_c is the normalized pixel intensity of color channel c , $N_{luminance}$ and $N_{chrominance}$ are random variables following a Normal distribution with mean $\mu = 0$ and standard deviation $\sigma = 1$, w_s is a weight factor, parameterized by severity level s .

PSF blur. Every optical system, *e.g.*, the lens array of a camera, exhibits optical aberrations. Many of them cause image blur. Point-spread-functions aggregate every optical aberration that results in blur. The point-spread-functions of an optical system are typically spatially-varying, meaning, for example, that the degree of blur is at the image edge more pronounced than in the center of the image. Figure A.4 illustrates the intensity distribution of a PSF kernel, where most of its energy is punctually centered.

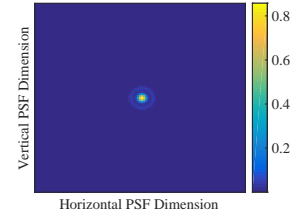


Figure A.4: The normalized intensity distribution of a PSF kernel of our proposed PSF blur.

Figure A.2 illustrates the intensity distribution of several PSF kernels utilized in the main paper. Each row corresponds to a specific PSF blur kernel at the respective angle of incidence, *i.e.*, the higher the angle of incidence, the higher the distance to the image center. Note that the PSF kernel varies its shape within a severity level (*i.e.*, column). The intensity of a PSF kernel is spatially more distributed for higher severity levels.

Geometric distortion. Distortion parameters of an optical system vary over time, are affected by environmental influences, differ from calibration stages, and thus, may never be fully compensated. Additionally, image warping may introduce re-sampling artifacts, degrading the informational content of an image. It can hence be preferable to utilize the original (*i.e.*, geometrically distorted) image [33, p.192f]. We used the command-line tool *ImageMagick* to apply a radially-symmetric barrel distortion as a polynomial of grade 4 to both the RGB and ground-truth images. It is essential to use the nearest-neighbor filter for color determination of the ground truth, as otherwise, the class labels are corrupted.

³<https://github.com/hendrycks/robustness/tree/master/ImageNet-C>

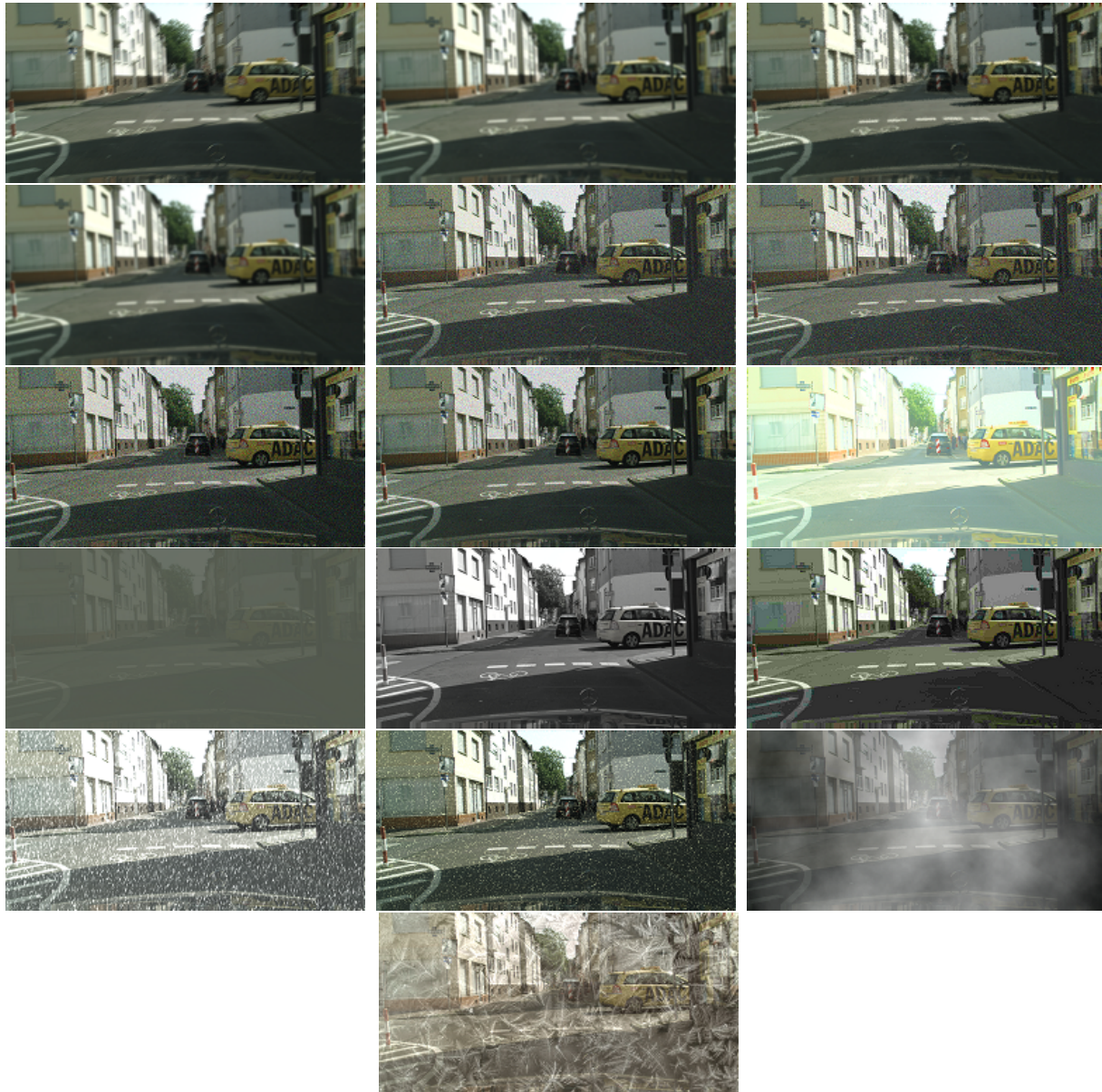


Figure A.1: Illustration of utilized image corruptions of ImageNet-C. First row: Motion blur, defocus blur, frosted glass blur. Second row: Gaussian blur, Gaussian noise, impulse noise. Third row: Shot noise, speckle noise, brightness. Fourth row: Contrast, saturate, JPEG. Fifth row: Snow, spatter, fog. Sixth row: frost.

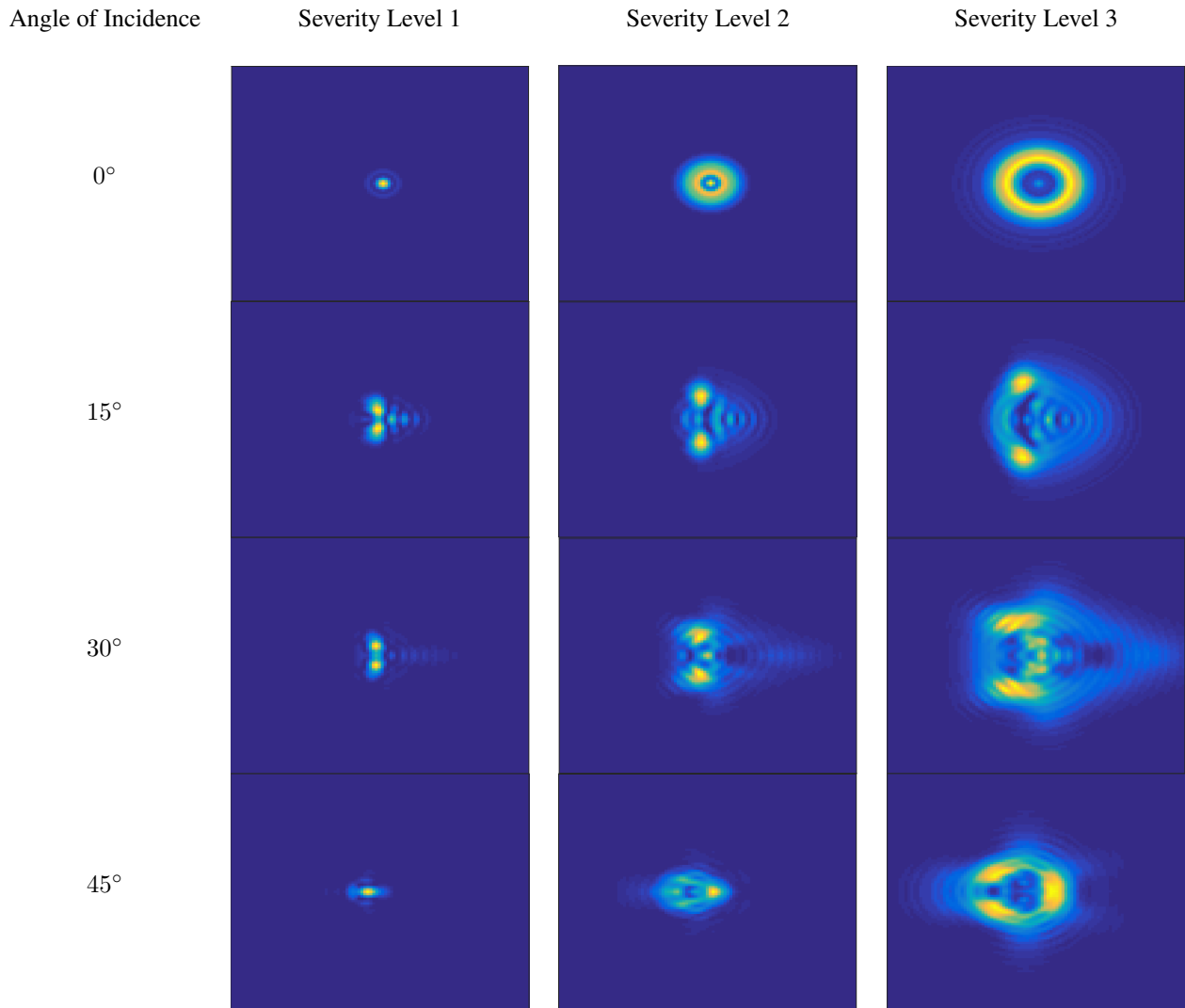


Figure A.2: The intensity distribution of used PSF kernels. The degree of the spatial distribution of intensity increases with the severity level. The shape of the PSF kernel depends on the image region, *i.e.*, the angle of incidence.



Figure A.3: Illustration of our proposed image corruptions. From left to right: Proposed noise model, PSF blur, and geometric distortion. Best viewed in color.

	Severity Level	Cityscapes	PASCAL VOC 2012	ADE20K
Gaussian Noise	1	13.2	18.6	18.3
	2	9.9	15.5	15.2
	3	6.8	12.4	12.1
	4	4.1	9.8	9.6
	5	1.7	7.3	7.3
Impulse Noise	1	11.2	16.7	16.5
	2	8.1	13.8	13.6
	3	6.4	12.1	12.0
	4	3.6	9.3	9.3
	5	1.6	7.2	7.4
Shot Noise	1	14.2	18.2	17.8
	2	10.5	14.9	14.3
	3	7.4	12.1	11.5
	4	3.9	8.9	8.2
	5	2.0	7.2	6.4
Speckle Noise	1	17.0	19.3	18.9
	2	14.5	17.1	16.6
	3	9.8	12.8	12.2
	4	7.9	11.0	10.3
	5	5.8	9.2	8.4
Intensity Noise	1	20.5	28.4	24.9
	2	18.6	22.1	23.1
	3	14.4	18.7	20.3
	4	10.8	15.1	15.5
	5	7.1	11.2	11.6

Table A.1: Averaged Signal-to-Noise ratios for corrupted variants of category image noise of the validation sets of Cityscapes, PASCAL VOC 2012, and ADE20K.

A.3. Signal-to-Noise Ratio for Image Corruptions

To make the severity levels of corruptions of category image noise mutually comparable, we provide in Tab. A.1 the SNR for this image corruption category.

B. Experiments

This section contains qualitative results and the remaining evaluation metric scores of the main paper. Based on DeepLabv3+, we evaluate the removal of atrous spatial pyramid pooling (ASPP), atrous convolutions (AC), and long-range link (LRL). We further replaced ASPP by Dense Prediction Cell (DPC) or applied global average pooling (GAP). Each ablated variant has been re-trained on the corresponding clean training data of Cityscapes, PASCAL VOC 2012, or ADE20K. To guarantee comparable results, we also re-trained the original, non-ablated models, though several publicly available checkpoints were available.

Besides DeepLabv3+, we have benchmarked several other semantic segmentation models as well.

B.1. Architectures

The DeepLabv3+ architecture functions⁴ as reference model in our ablation study. We have benchmarked many other semantic segmentation models, such as FCN8s-VGG16 (trained by us), ICNet⁵, DilatedNet⁶, ResNet-38⁷, PSPNet⁸, and the recent Gated-ShapeCNN (GSCNN)⁹, using mostly publicly available model checkpoints. Regarding PSPNet and ICNet, we conducted the benchmark using a PyTorch [64, 72] implementation¹⁰.

B.2. Experimental Details

Hardware Setup. We have trained the models on machines equipped with four GTX 1080 Ti, each having 11 GB of memory or on a machine with two Titan RTX, each having 24 GB of memory.

Training Details. We set the crop size in every training for every dataset to 513, used a batch size of 16, as we always fine-tuned the batch normalization parameters. We applied the original training protocol of the developers of DeepLabv3+. We applied a polynomial learning rate with an initial learning rate of 0.007 or 0.01.

We re-trained 102 models for this benchmark: On ADE20K and the Cityscapes dataset, we re-trained 36 models each (six architectural ablations per network backbone; six network backbones in total). On PASCAL VOC, we re-trained 30 models, as we have evaluated on one network backbone less than on Cityscapes and ADE20K.

B.3. Evaluation Metrics

In the main paper, we predominantly use the Corruption Degradation (CD) to rate model robustness with respect to image corruptions, since the CD rates model robustness in terms of absolute performance. The relative Corruption Degradation (rCD), on the other hand, incorporates the respective model performance on clean data. The degradation on clean data is for both models (i.e., the model for which the robustness is to be rated, and the reference model) subtracted, resulting hence in a measure that gives a ratio of the absolute performance decrease in the presence of image corruption.

B.4. Discussion of Architectural Properties

As mentioned in the main paper, we now discuss possible causes of the robustness of architectural design choices with respect to image corruptions in more detail.

⁴<https://github.com/tensorflow/models/tree/master/research/deeplab>

⁵<https://github.com/hszhao/ICNet>

⁶<https://github.com/fyu/dilation>

⁷<https://github.com/itijyou/ademxapp>

⁸<https://github.com/hszhao/PSPNet>

⁹<https://github.com/nv-tlabs/GSCNN>

¹⁰<https://github.com/meetshah1995/pytorch-semseg>

Dense Prediction Cell. As mentioned in the main paper, a model with Dense Prediction Cell (DPC) might learn less multi-scale representations than a model with the Atrous Spatial Pyramid Pooling (ASPP) module. Whereas ASPP processes its input in parallel by three atrous convolution (AC) layers with large symmetric rates (6, 12, 18), DPC firstly processes the input by a single AC layer with small rate (1×6) [10, Fig. 5]. We hypothesize that DPC might learn less multi-scale representations than ASPP, which may be useful for common image corruptions (e.g., [26] shows that classification models are more robust to common corruption if the shape bias of a model is increased). When we test DPC on corrupted data, it cannot hence apply the same beneficial multi-scale cues (due to the comparable small atrous convolution with rate 1×6) as ASPP and may, therefore, perform worse.

Global Average Pooling. Global average pooling (GAP) increases performance on clean data on PASCAL VOC 2012, but not on the Cityscapes dataset or ADE20K. GAP averages 2048 activations of size 33×33 for our utilized training parameters. A possible explanation for the effectiveness of GAP on PASCAL VOC 2012 might be, that the Cityscapes dataset and ADE20K consist of both a notably larger number and spatial distribution of instances per image. Using GAP on these datasets might therefore not aid performance since important features may be lost due to averaging.

Long-Range Link. Removing the Long-Range Link (LRL) discards early representations. The degree of, e.g., image noise is more pronounced on early CNN levels. Removing LRL tends hence to increase the robustness for a more shallow backbone as Xception-41 on PASCAL VOC 2012 and Cityscapes, as less corrupted features are linked from encoder to decoder. For a deeper backbone like ResNet-101, this behavior cannot be observed.

B.5. Qualitative Results

We provide qualitative results in this subsection. As mentioned in the main paper, blurred images cause the models to miss-classify pixels of classes covering small image regions, especially when far away. Please see Figure B.1 for an example. (a) A blurred validation image of the Cityscapes dataset and the corresponding ground truth in (b). (c) The prediction on the clean image overlaid with the ground truth (b). In this visualization, true-positives are alpha-blended, and false-positives, as well as false-negatives, remain unchanged. Hence, wrongly classified pixels can be easier identified. (d) The prediction on the blurred image overlaid with the ground truth (b). Whereas the *riders* and *persons* are mostly correctly classified in (c), *riders* in (d) are miss-classified as *persons*, and extensive areas of *road* are miss-classified as *sidewalk*. We used the reference model along with Xception-71 as network back-

bone to produce these predictions.

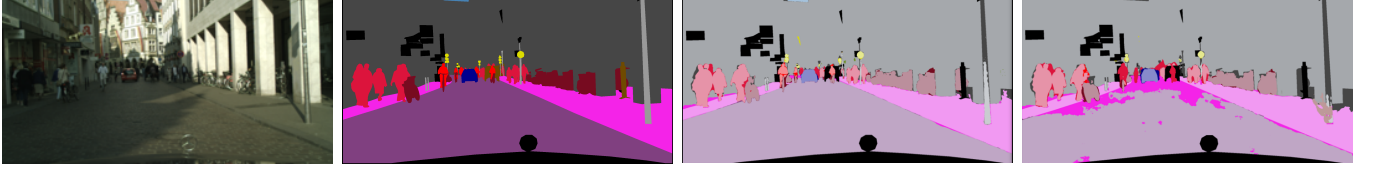
We report in the main paper, that—of the utilized image corruptions in this work—image noise affects model performance the most, as pointed out using mIoU scores. To give a visual example, we selected two noisy variants of a validation image of the Cityscapes dataset and show the predictions of the reference architecture using Xception-71 as network backbone in Figure B.2. The mIoU for both predictions is less than 15 %.

Finally, we show qualitative results of every ablated architecture for one image corruption of category blur, noise, digital, and weather. Figure B.3 shows a blurred validation image of the Cityscapes dataset and the corresponding predictions. Note that the ablated variants w/o AC and w/ DPC are especially vulnerable. Figure B.4 shows a noisy validation image of the Cityscapes dataset. Note that the ablated variants w/o AC, w/o ASPP and w/ DPC are especially vulnerable. Figure B.5 and Figure B.6 show a validation image of PASCAL VOC 2012, corrupted by *brightness* and *snow*, respectively.

B.6. Experimental Results on Cityscapes

In this section, we provide a more detailed analysis of both the non-Deeplabv3+ and Deeplabv3+ based segmentation models. Figure B.7 illustrates the CD and rCD averaged for the proposed image corruption categories. Please note that the CD of image corruption “jpeg compression” of category digital is not included in this barplot. Contrary to the remaining image corruptions of that category, the respective CDs are considerably high (see Tab. B.1). FCN8s-VGG16 and DilatedNet are vulnerable to blur. The CD of *defocus blur* 124 % and 115 %, respectively. However, DilatedNet is more robust against corruptions of category noise, digital, and weather than ICNet. For example, the CD of *intensity noise* is 92 %. ResNet-38 is robust against corruptions of category weather. Both the CD and rCD for *fog* are roughly 65 %. The CD of PSPNet is oftentimes less than 100 % (see Table B.1). GSCNN performs very well on digital corruptions (except *JPEG compression*) and weather corruptions, especially *fog* (CD is 44 %, rCD is 34 %). The model is, however, vulnerable to image noise, as CD and rCD are always higher than 100 %. We list the individual CD and rCD scores in Table B.1. Please find the absolute mIoU values in Table 1 (bottom) in the main paper.

Table B.2 contains the mIoU for clean and corrupted variants of the validation set of the Cityscapes dataset for several network backbones of the Deeplabv3+ architecture and each respective architectural modification. In addition to the main paper, where we discuss the CD score (see Figure 5 in the main paper), Figure B.9 illustrates the rCD (see equation 2 in the main paper) for each ablated variant evaluated on the Cityscapes dataset. In the following, we briefly discuss the ablated variants w.r.t. rCD.



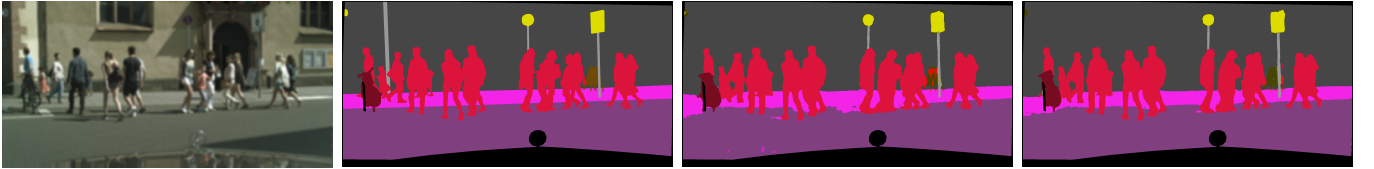
(a) Blurred validation image (b) ground truth (gt) (c) Overlay clean estimate + gt (d) Overlay blurred estimate + gt

Figure B.1: Prediction of the reference architecture (*i.e.* original DeepLabv3+) on blurred input, using Xception-71 as network backbone. (a) A blurred validation image of the Cityscapes dataset and corresponding ground truth (b). (c) Prediction on the clean image overlaid with the ground truth. True-positives are alpha-blended, false-positives and false-negatives remain unchanged. Hence, wrongly classified pixels can be easier spotted. (d) Prediction on the blurred image overlaid with the ground truth (b). Whereas the *riders* are mostly correctly classified in (c), they are in (d) miss-classified as *person*. Extensive areas of *road* are miss-classified as *sidewalk*.

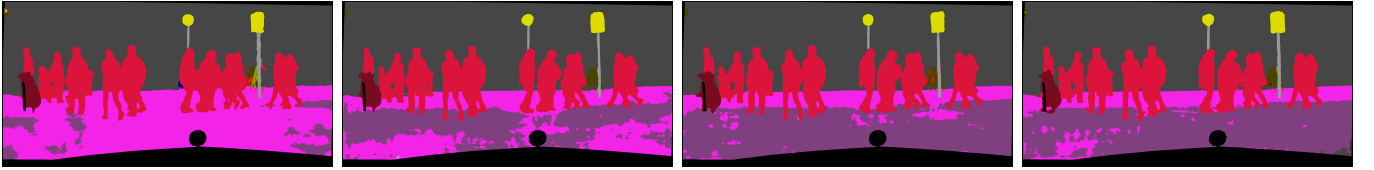


(a) Corrupted validation image (b) Prediction on (a) (c) Corrupted validation image (d) Prediction on (c)

Figure B.2: Drastic influence of image noise on model performance. (a) A validation image of Cityscapes is corrupted by the second severity level of Gaussian noise and respective prediction (b). (c) A validation image of Cityscapes is corrupted by the third severity level of Gaussian Noise and respective prediction (d). Predictions are produced by the reference model, using Xception-71 as the backbone.

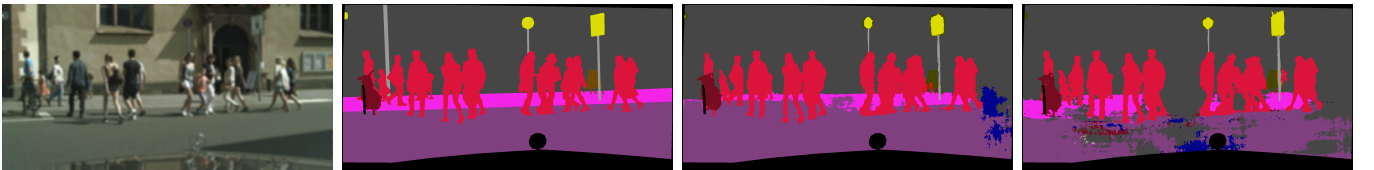


(a) corrupted image (b) ground truth (c) prediction of ref. model (d) prediction w/o ASPP

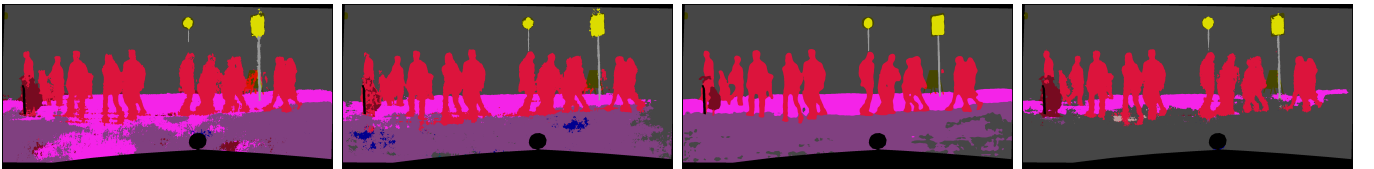


(e) prediction w/o AC (f) prediction w/ DPC (g) prediction w/o LRL (h) prediction w/ GAP

Figure B.3: Predictions of reference architecture and ablations on a blurred image. The ablated variants w/o AC, and w/ DPC are especially vulnerable to blur.



(a) corrupted image (b) ground truth (c) prediction of ref. model (d) prediction w/o ASPP



(e) prediction w/o AC (f) prediction w/ DPC (g) prediction w/o LRL (h) prediction w/ GAP

Figure B.4: Predictions of reference architecture and ablations on a noisy image. The ablated variants w/o AC, ASPP, and w/ DPC, GAP are especially vulnerable.

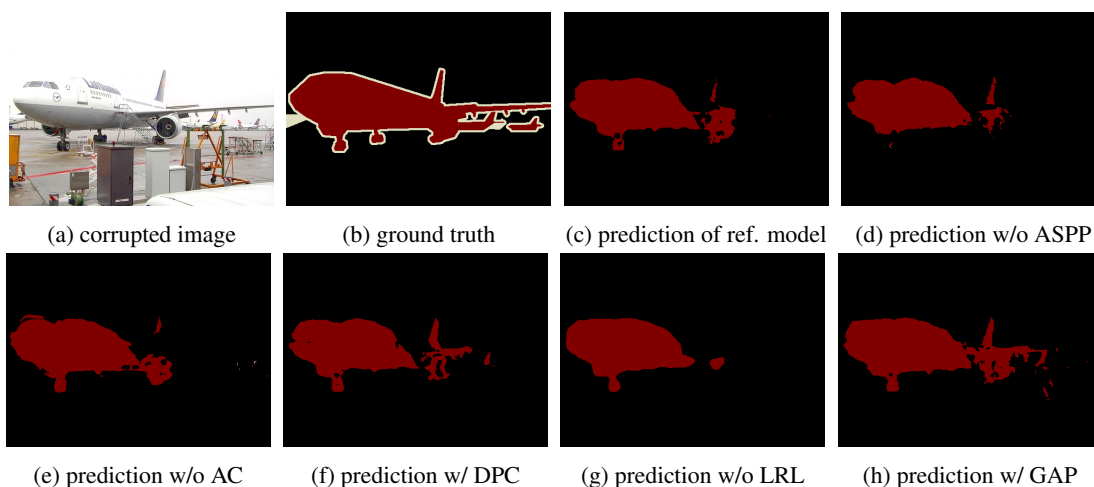


Figure B.5: Predictions of reference architecture and ablations on a validation image of PASCAL VOC 2012, corrupted by *brightness*.

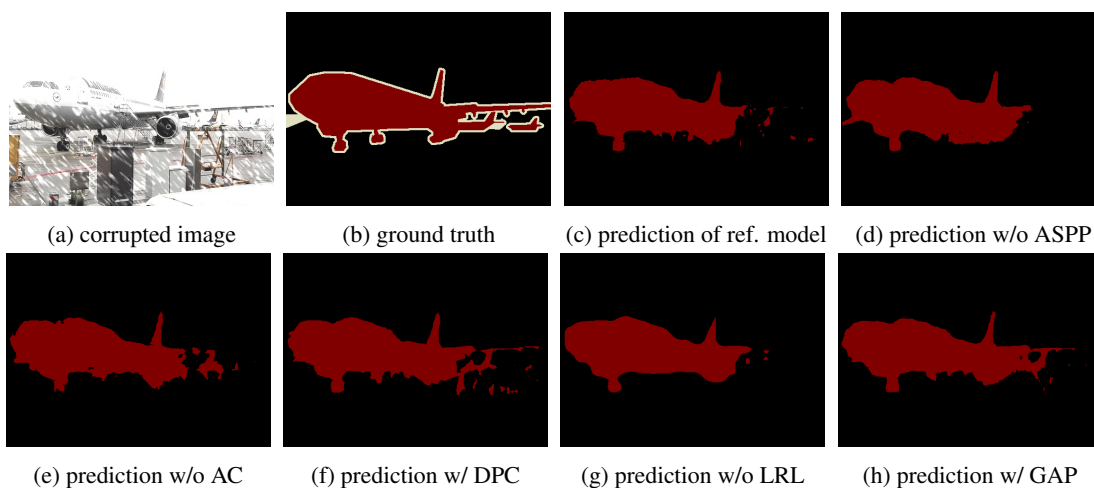


Figure B.6: Predictions of the reference architecture and ablations on a validation image of PASCAL VOC 2012, corrupted by *snow*.

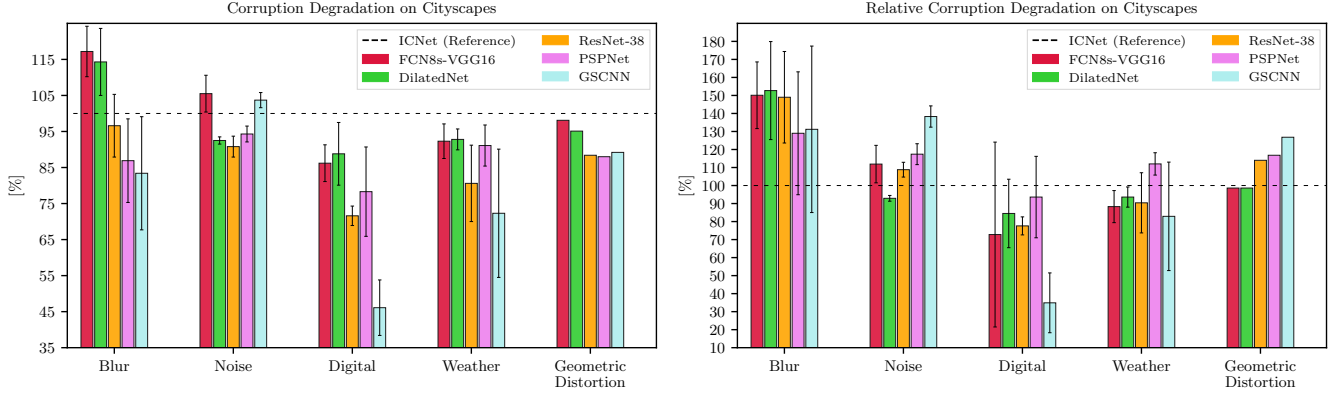


Figure B.7: CD (left) and rCD (right) evaluated on Cityscapes for ICNet (set as reference architecture), FCN8s-VGG16, DilatedNet, ResNet-38, PSPNet, GSCNN w.r.t. image corruptions of category blur, noise, digital, weather, and geometric distortion. Each bar except for geometric distortion is averaged within a corruption category (error bars indicate the standard deviation). The CD of image corruption “jpeg compression” of category digital is not included in this barplot, since, contrary to the remaining image corruptions of that category, the respective CDs range between 107 % and 133 %. Bars above 100 % represent a decrease in performance compared to the reference architecture. FCN8s-VGG16 and DilatedNet are vulnerable to corruptions of category blur. DilatedNet is more robust against corruptions of category noise, digital, and weather than the reference. ResNet-38 is robust against corruptions of category weather. The rCD of PSPNet is oftentimes higher than 100 % for each category. GSCNN is vulnerable to image noise. The rCD is considerably high, indicating a high decrease of mIoU in the presence of this corruption. Best viewed in color.

Effect of ASPP. The rCD score is especially pronounced for geometrically distorted image data (146 % for Xception-41, 46 % for MobileNet-V2). The mIoU of Xception-41 on geometrically distorted data is low, resulting hence in a high CD and rCD. Regarding MobileNet-V2, the averaged mIoU is even similar to the other ablated variants (see the last column of Table B.2).

Effect of AC. As discussed in the main paper, AC show often an aiding effect against corruptions of type blur, noise, and geometric distortion (especially for ResNets and Xception-71). The rCD mostly has a similar tendency as the CD.

Effect of DPC. The rCD scores for the ablated variant without ASPP and with Dense Prediction Cell, generally show the same tendency as the CD illustrated in the main paper in Figure 5.

Effect of LRL. As mentioned in the main paper, this ablated variant is vulnerable to *intensity noise (defocus blur)*, when applied in ResNet-101 (MobileNet-V2), since its rCD is 124 % (118 %). The rCD with respect to geometric distortion is especially high for MobileNet-V2 (155 %).

Effect of GAP. The rCD of Xception-71 and ResNet-101, using GAP, show a similar tendency as the CD discussed in the main paper. The rCD is low for Xception-71 w.r.t. geometric distortion.

Finally, we list for completeness the individual CD and rCD scores, evaluated on Cityscapes, in Table B.3 and Table B.4.

B.7. Experimental Results on PASCAL VOC 2012

Table B.5 contains the mIoU for clean and corrupted variants of the validation set of PASCAL VOC 2012 for several network backbones of the DeepLabv3+ architecture. In contrast to the model performance evaluated on Cityscapes, corruptions of category noise and weather have a less corrupting impact. Each backbone performs best on clean data when GAP is used. Each backbone performs significantly worse without ASPP. When GAP is used with ResNets and Xception-65, the resulting model is the best performing model on most types of image corruptions. Regarding Xception-41 and Xception-71, the ablated variant without LRL often has the highest mIoU w.r.t. image corruptions of category noise. Figure B.10 and Figure B.11 illustrates the CD and rCD for each ablated variant evaluated on PASCAL VOC 2012. In the following, we will briefly discuss the ablated variants w.r.t. rCD.

Effect of ASPP. For geometric distortion, the rCD of this ablated variant often shows except for Xception-41 a similar tendency the rCD as on Cityscapes (see Figure B.9). The rCD for ranges from 24 % (ResNet-101) to 62 % (Xception-65).

Effect of AC. As mentioned in the main paper, AC show no positive effect against blur. We explain this with the fundamentally different datasets. On Cityscapes, a model without AC often overlooks classes covering small image-regions, especially when far away. Such images are hardly present in PASCAL VOC 2012. An example of Cityscapes is illustrated in Figure B.1. The tendencies of CD and rCD are often similar to geometric distortion. As on Cityscapes,

AC aids the robustness for ResNet-101 against this image corruption, but not for ResNet-50.

Effect of DPC. The harming effect of DPC with respect to image corruptions is especially present for Xception-71. As mentioned in the main paper, a possible explanation might be that the neural-architecture-search has been performed on Xception-71.

Effect of LRL. The rCD for this ablated variant is especially high w.r.t. geometrically distorted image data when applied in Xception-41 and ResNet-50 (144 % and 127 %, respectively). As the CD reported in the main paper, also the rCD of Xception-71 and Xception-41 for image noise is below 100 %.

Effect of GAP. Unlike the tendency of CD, the rCD of this ablated variant is rarely below 100.0 %. The rCD w.r.t. is high for geometric distortion.

Finally, we list the individual CD and rCD scores, evaluated on PASCAL VOC 2012, in Table B.6 and Table B.7.

B.8. Experimental Results on ADE20K

Table B.8 contains the mIoU for clean and corrupted variants of the validation set of ADE20K for several network backbones of the DeepLabv3+ architecture. When comparing the respective reference model of each backbone (*i.e.* no ablated variants), Xception-71 performs best for every type of image corruption. MobileNet-V2 (ResNets) oftentimes performs best when DPC (GAP) is used. Xception-41 and Xception-71 perform best on clean data when DPC is used. Most backbones without ASPP perform significantly worse than respective reference. Figure B.12 and Figure B.13 illustrates the CD and rCD for each ablated variant evaluated on ADE20K. As mentioned in the main paper, the CD is—except for models without ASPP—oftentimes around 100 %. In the following, we will briefly discuss the ablated variants w.r.t. CD and rCD.

Effect of ASPP. The rCD is in general above 100 % for both Xception-65 and Xception-71, and below 100 % for remaining backbones. The performance gap w.r.t. the reference model is for the aforementioned Xception-based backbones significantly less than for the remaining backbones.

Effect of AC. The removal of AC decreases the performance slightly for most backbones against corruptions of category digital and weather.

Effect of DPC. As on PASCAL VOC 2012 and Cityscapes, applying DPC oftentimes decreases the robustness, especially for Xception-71 against most image corruptions. As on Cityscapes, using DPC along Xception-71, results in the best-performing model on clean data.

Effect of LRL. The removal of LRL impacts especially Xception-71 against image noise.

Effect of GAP. When GAP is applied, the models perform generally most robust.

Finally, we list the individual CD and rCD scores, eval-

uated on ADE20K, in Table B.9 and Table B.10.

B.9. Performance without ASPP

As mentioned in the main paper, we provide a more detailed evaluation for the ablated architecture without ASPP for every dataset, in this subsection. The Atrous Spatial Pyramid Pooling (ASPP) module reduces, in general, the model performance significantly. On PASCAL VOC 2012, the mIoU on clean data reduces between 5.9 % (Xception-65) and 12.0 % (ResNet-50). On ADE20K, the mIoU decreases between 1.2 % (Xception-65) and 7.7 % (ResNet-50). On Cityscapes, the mIoU decreases between 2.4 % (Xception-41) and 7.1 % (MobileNet-V2). Therefore, the corresponding CD scores are oftentimes considerably high. On PASCAL VOC 2012 and ADE20K, for example, the CD score for the ablated variant w/o ASPP is the highest w.r.t. every image corruption and for every network backbone (see bold values Table B.6 and Table B.9). Regarding the evaluation on Cityscapes (see Table B.3), the CD score of the ablated variant w/o ASPP is often high against image corruptions of category blur for ResNets and MobileNet-V2. Stronger backbones, on the other hand, as Xception-based ones, perform better without ASPP and have thus a lower CD.

B.10. Performance with respect to Individual Severity Levels

We illustrate in Fig. B.8 the model performance evaluated on every dataset with respect to individual severity levels. The Figure shows the degrading performance with increasing severity level for some candidates of category blur, noise, digital, and weather of a reference model and all corresponding architectural ablations. Please see the caption for discussion.

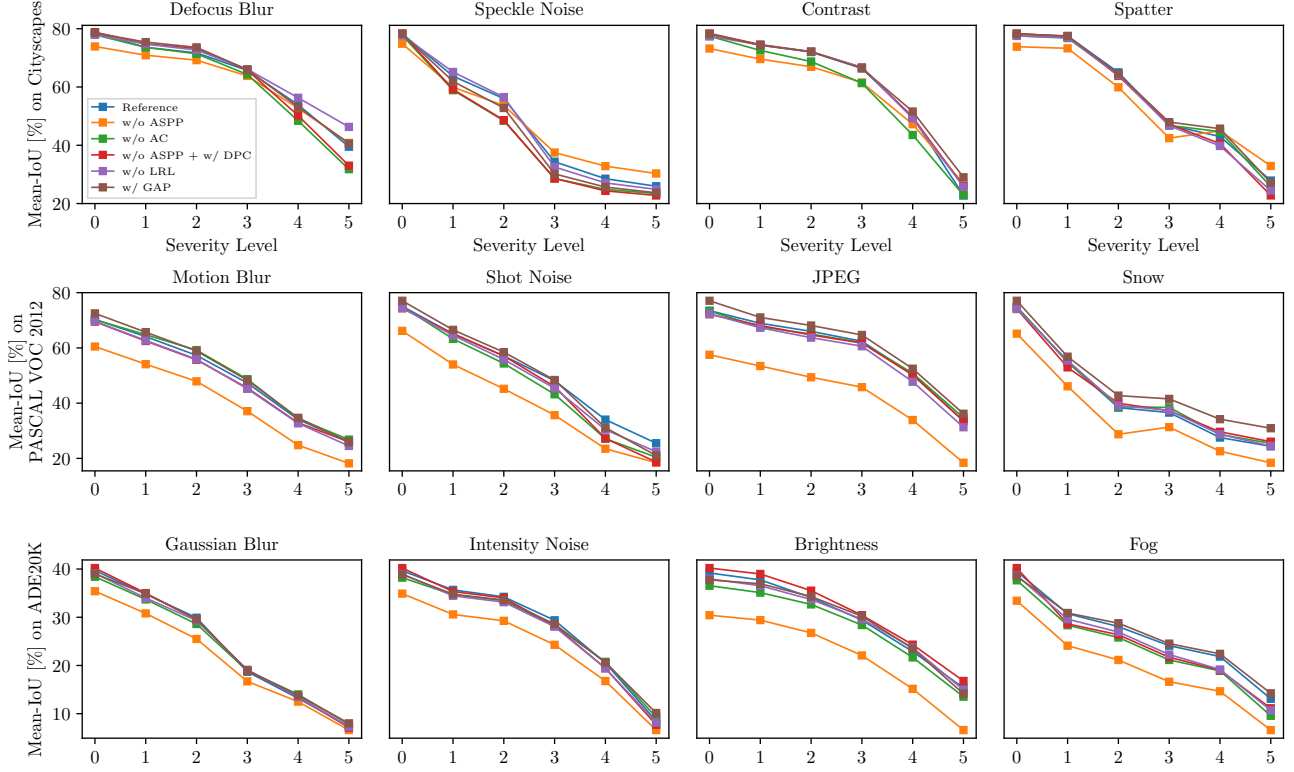


Figure B.8: Model performance (mIoU) for many candidates with respect to the image corruption categories blur (first column), noise (second column), digital (third column), and weather (fourth column) for a reference model and all corresponding architectural ablated variants, evaluated for every severity levels on Cityscapes, PASCAL VOC 2012, and ADE20K. Severity level 0 corresponds to clean data. **First row:** Xception-71 evaluated on the Cityscapes dataset for defocus blur, speckle noise, contrast, and spatter. **Second row:** ResNet-101 evaluated on PASCAL VOC 2012 for motion blur, shot noise, JPEG, and snow. **Third row:** Xception-41 evaluated on ADE20K for Gaussian blur, intensity noise, brightness, and fog. The ablated variant without ASPP oftentimes has the lowest mIoU. However, it performs best on speckle noise for severity level 3 and above. The mIoU of the ablated variant without AC is relatively low for defocus blur and contrast. The mIoU of the ablated variant without ASPP and with DPC is relatively low for speckle noise, shot noise (for severity level 4 and 5), spatter. The mIoU of the ablated variant without LRL is relatively high for speckle noise and shot noise. The mIoU of the ablated variant with GAP is high for PASCAL VOC 2012 on clean data and low for speckle noise.

Deeplab-v3+ Backbone	Blur					Noise					Digital				Weather				Geometric Distortion
	Motion	Defocus	Frosted Glass	Gaussian	PSF	Gaussian	Impulse	Shot	Speckle	Intensity	Brightness	Contrast	Saturate	JPEG	Snow	Spatter	Fog	Frost	
ICNet	100.0	100.0	100.0	100.0	100.0	100.0	100.0	100.0	100.0	100.0	100.0	100.0	100.0	100.0	100.0	100.0	100.0	100.0	100.0
FCN8s-VGG16	105.6	124.3	119.6	119.1	110.8	101.8	103.0	103.2	104.1	115.6	79.2	91.2	88.2	119.4	94.7	98.4	85.8	90.2	98.1
DilatedNet	102.6	115.1	128.3	111.4	111.8	92.2	93.9	91.3	93.3	91.9	80.2	100.7	85.4	107.3	93.4	97.3	89.8	90.7	95.1
ResNet-38	83.7	99.2	107.8	95.5	72.0	94.3	91.8	91.5	85.5	91.2	67.8	73.8	73.3	129.2	92.4	77.9	64.7	87.4	88.4
PSPNet	74.1	84.6	105.7	83.3	66.3	97.1	92.4	94.7	91.1	96.2	67.1	72.1	95.7	119.1	97.8	82.5	90.2	94.1	88.0
GSCNN	75.9	75.1	110.4	72.2	56.5	103.2	106.4	104.3	104.4	100.0	40.9	57.0	40.4	133.2	93.5	75.8	44.1	75.7	89.2
ICNet	100.0	100.0	100.0	100.0	100.0	100.0	100.0	100.0	100.0	100.0	100.0	100.0	100.0	100.0	100.0	100.0	100.0	100.0	100.0
FCN8s-VGG16	119.1	167.3	160.1	153.8	779.8	104.3	106.1	106.6	109.9	132.5	54.0	84.6	79.9	142.7	93.1	99.1	75.3	85.5	98.6
DilatedNet	120.5	152.2	195.4	142.8	1117.9	92.3	95.0	90.8	94.4	91.8	64.0	109.9	79.5	123.8	94.3	102.5	87.8	89.9	98.6
ResNet-38	114.2	152.9	185.3	143.5	388.9	111.2	107.2	107.4	103.1	115.2	70.6	82.1	80.0	197.2	107.7	89.5	63.7	100.8	114.0
PSPNet	93.7	120.0	185.3	116.8	256.0	117.7	110.2	114.6	116.8	127.9	73.5	82.1	125.2	179.7	117.9	101.7	114.7	113.7	116.8
GSCNN	109.7	105.9	211.0	98.3	85.1	131.2	136.4	134.2	147.9	141.6	20.2	58.1	26.5	216.0	115.0	95.0	33.7	87.9	126.8

Table B.1: CD (top) and rCD (bottom) for corrupted variants of the validation set of the Cityscapes dataset for several non-Deeplabv3+ based architectures. ICNet is used as reference model. Highest CD and rCD per corruption is bold.

DeepLab-v3+ Backbone	Blur						Noise					Digital				Weather				Geometric Distortion
	Clean	Motion	Defocus	Frosted Glass	Gaussian	PSF	Gaussian	Impulse	Shot	Speckle	Intensity	Brightness	Contrast	Saturate	JPEG	Snow	Spatter	Fog	Frost	
MobileNet-V2	72.0	53.5	49.0	45.3	49.1	70.5	6.4	7.0	6.6	16.6	26.9	51.7	46.7	32.4	27.2	13.7	38.9	47.4	17.3	65.5
w/o ASPP	64.9	45.5	40.4	39.0	41.5	63.3	7.7	8.7	8.9	19.9	28.4	41.7	36.1	27.6	20.7	13.0	36.8	37.8	14.0	61.9
w/o AC	71.2	52.1	49.1	42.8	49.3	69.8	3.6	7.2	4.5	19.6	29.2	49.8	46.2	31.4	28.1	10.0	44.6	45.2	16.7	63.5
w/ DPC	71.6	49.4	42.2	43.7	43.8	69.2	3.5	4.9	3.9	16.1	27.4	45.0	38.6	30.1	24.1	9.8	42.8	43.9	14.0	62.2
w/o LRL	71.1	49.7	43.9	44.4	45.1	68.9	1.9	2.6	2.5	19.6	26.6	49.1	43.5	32.2	26.3	10.4	39.5	44.9	14.7	60.9
w/ GAP	71.4	52.2	50.6	43.3	51.8	69.8	8.5	10.9	10.8	26.0	32.5	51.8	47.3	35.3	25.7	12.7	43.4	45.1	12.6	66.0
ResNet-50	76.6	58.5	56.6	47.2	57.7	74.8	6.5	7.2	10.0	31.1	30.9	58.2	54.7	41.3	27.4	12.0	42.0	55.9	22.8	69.5
w/o ASPP	71.4	52.3	50.7	41.2	52.0	69.7	10.1	11.3	13.8	31.2	33.3	50.2	48.4	37.0	25.3	12.0	38.6	42.7	18.7	65.9
w/o AC	76.0	56.7	53.1	47.3	54.1	73.8	2.4	6.1	5.1	25.5	25.7	56.8	51.4	38.9	27.6	9.7	40.8	52.0	20.1	66.9
w/ DPC	76.9	57.0	54.7	46.9	56.2	74.2	10.7	12.6	13.6	33.1	32.0	54.5	53.6	41.5	25.1	11.4	41.3	56.3	20.4	68.6
w/o LRL	75.6	57.9	54.4	46.4	55.6	73.8	7.9	9.3	11.2	31.8	34.7	56.2	51.6	40.2	28.5	11.9	41.4	55.4	21.1	67.9
w/ GAP	76.5	56.7	55.7	45.8	57.4	75.2	5.5	7.8	9.5	31.3	34.5	57.7	51.4	41.1	28.3	10.5	40.4	54.5	20.1	68.5
ResNet-101	77.1	59.1	56.3	47.7	57.3	75.2	13.2	13.9	16.3	36.9	39.9	59.2	54.5	41.5	37.4	11.9	47.8	55.1	22.7	69.7
w/o ASPP	71.1	53.8	50.6	42.2	51.7	68.8	9.5	9.8	12.7	30.7	32.5	52.1	48.3	36.7	33.2	13.3	43.5	47.8	23.2	66.4
w/o AC	75.7	57.9	52.5	46.6	53.9	73.3	8.4	11.0	11.6	31.5	28.8	53.5	53.1	39.1	34.2	9.9	44.7	55.0	20.0	65.5
w/ DPC	77.0	58.5	53.5	46.7	54.8	75.3	11.7	12.1	15.6	36.4	35.5	53.7	54.3	39.8	30.9	10.1	44.0	56.0	19.3	68.6
w/o LRL	76.5	58.7	54.6	47.5	55.7	74.3	9.1	8.3	12.1	33.5	30.3	57.0	57.6	40.9	35.7	9.3	44.3	55.4	20.8	69.2
w/ GAP	77.3	58.7	56.9	48.4	57.8	75.9	8.2	7.4	11.6	32.0	32.8	55.6	55.8	39.3	36.4	11.5	44.8	52.5	22.6	69.0
Xception-41	77.8	61.6	54.9	51.0	54.7	76.1	17.0	17.3	21.6	43.7	48.6	63.6	56.9	51.7	38.5	18.2	46.6	57.6	20.6	73.0
w/o ASPP	75.4	59.7	55.5	47.4	55.4	73.1	15.1	14.4	19.7	40.7	43.6	60.4	52.5	46.8	37.0	18.0	47.2	52.4	22.1	68.4
w/o AC	77.4	62.2	55.6	51.3	54.5	75.4	17.7	15.7	22.1	42.8	46.5	61.6	54.9	47.8	34.3	17.8	46.6	59.1	20.9	70.9
w/ DPC	77.5	60.6	53.0	50.8	52.5	75.8	15.1	10.7	20.3	42.7	48.4	63.6	53.4	46.0	36.0	17.6	50.0	56.7	20.6	71.8
w/o LRL	76.8	62.3	53.2	50.6	53.0	75.1	21.3	19.2	27.6	49.3	51.7	63.9	55.2	48.0	33.8	20.5	48.3	57.6	23.9	70.8
w/ GAP	77.1	61.5	54.8	53.1	53.9	75.6	20.0	16.4	24.8	43.4	46.6	65.7	57.6	50.4	36.2	16.5	48.6	56.8	22.6	72.5
Xception-65	78.4	63.9	59.1	52.8	59.2	76.8	15.0	10.6	19.8	42.4	46.5	65.9	59.1	46.1	31.4	19.3	50.7	63.6	23.8	72.7
w/o ASPP	75.8	61.6	56.1	51.8	54.6	74.1	14.3	7.7	18.8	39.0	41.6	62.0	57.2	43.1	29.7	15.6	46.9	60.3	23.4	70.6
w/o AC	77.7	63.9	58.7	51.5	57.8	75.7	14.1	14.8	19.5	41.9	45.1	63.9	58.3	42.9	35.0	15.7	51.4	60.9	21.4	71.8
w/ DPC	77.7	62.4	55.0	50.4	54.5	74.7	8.9	4.8	13.2	37.1	47.7	62.5	48.4	45.4	30.3	17.3	47.1	59.6	21.9	70.7
w/o LRL	77.7	64.5	58.6	49.5	57.9	75.9	15.1	12.0	19.9	42.1	45.9	63.8	57.9	46.1	35.9	18.4	46.3	63.5	22.0	71.4
w/ GAP	78.4	63.9	59.4	53.5	58.8	76.2	18.8	15.4	23.7	43.7	45.7	65.2	56.5	48.0	31.5	18.8	49.4	59.1	20.7	71.0

Table B.2: Mean IoU for clean and corrupted variants of the validation set of the Cityscapes dataset for several network backbones of the DeepLabv3+ architecture and respective architectural ablations. Every mIoU is averaged over all available severity levels, except for corruptions of category noise where only the first three severity levels are considered. The standard deviation for image corruptions of category noise is 0.2 or less. Highest mIoU per corruption is bold.

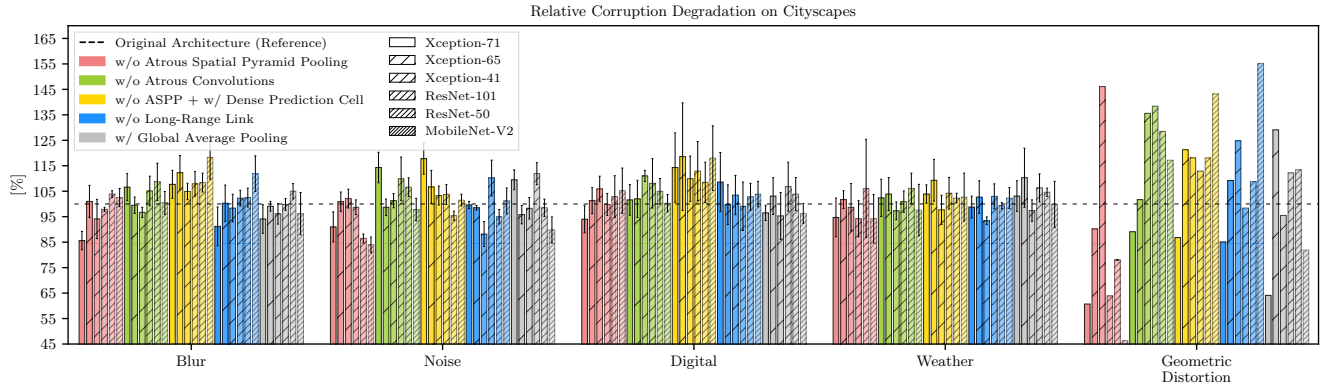


Figure B.9: Relative CD evaluated on Cityscapes for the proposed ablated variants of the DeepLabv3+ architecture w.r.t. image corruptions, employing six different network backbones. Each bar except for geometric distortion is averaged within a corruption category (error bars indicate the standard deviation). Bars above 100 % represent a relative decrease in performance compared to the respective reference architecture. Each ablated architecture is re-trained on the original training dataset. Removing ASPP may decrease performance significantly. The low rCD for geometric distortion indicates that the relative decrease of performance for this ablated variant is low. AC affect model performance, particularly against geometric distortion. The relative CD is often high against most image corruptions when DPC is used. The effect of GAP depends strongly on the network backbone. Best viewed in color.

Deeplab-v3+ Backbone	Blur					Noise					Digital				Weather				Geometric Distortion
	Motion	Defocus	Frosted Glass	Gaussian	PSF	Gaussian	Impulse	Shot	Speckle	Intensity	Brightness	Contrast	Saturate	JPEG	Snow	Spatter	Fog	Frost	
MobileNet-V2	100.0	100.0	100.0	100.0	100.0	100.0	100.0	100.0	100.0	100.0	100.0	100.0	100.0	100.0	100.0	100.0	100.0	100.0	100.0
w/o ASPP	117.2	116.8	111.5	115.0	124.2	98.6	98.1	97.6	96.1	97.9	120.6	120.0	107.1	109.0	100.7	103.5	118.2	104.0	110.4
w/o AC	103.1	99.9	104.6	99.8	102.2	103.0	99.7	102.2	96.4	96.9	104.0	101.1	101.5	98.8	104.2	90.8	104.1	100.7	105.7
w/ DPC	108.9	113.4	102.9	110.4	104.2	103.1	102.3	102.9	100.6	99.3	113.9	115.3	103.4	104.3	104.5	93.7	106.7	103.9	109.4
w/o LRL	108.2	110.0	101.7	108.0	105.3	104.8	104.8	104.4	96.3	100.0	105.5	106.1	100.3	101.2	103.8	99.1	104.8	103.1	113.2
w/ GAP	102.8	96.9	103.6	94.8	102.2	97.7	95.8	95.5	88.7	92.3	99.9	98.9	95.7	102.1	101.1	92.8	104.3	105.6	98.4
ResNet-50	100.0	100.0	100.0	100.0	100.0	100.0	100.0	100.0	100.0	100.0	100.0	100.0	100.0	100.0	100.0	100.0	100.0	100.0	100.0
w/o ASPP	115.1	113.6	111.3	113.5	120.3	96.2	95.5	95.8	99.9	96.4	119.0	113.9	107.3	102.9	100.1	105.8	130.1	105.3	111.8
w/o AC	104.4	108.1	99.7	108.5	104.2	104.3	101.2	105.4	108.1	107.5	103.2	107.4	104.1	99.8	102.6	102.0	109.0	103.5	108.6
w/ DPC	103.6	104.3	100.5	103.7	102.3	95.5	94.2	96.0	97.1	98.3	108.6	102.4	99.7	103.3	100.7	101.0	99.1	103.1	103.0
w/o LRL	101.5	104.9	101.5	105.1	104.2	98.5	97.7	98.6	99.1	94.4	104.6	106.8	101.8	98.5	100.1	101.0	101.3	102.2	105.1
w/ GAP	104.3	102.1	102.7	100.7	98.3	101.1	99.3	100.6	99.7	94.7	101.2	107.3	100.3	98.8	101.8	102.8	103.3	103.4	103.2
ResNet-101	100.0	100.0	100.0	100.0	100.0	100.0	100.0	100.0	100.0	100.0	100.0	100.0	100.0	100.0	100.0	100.0	100.0	100.0	100.0
w/o ASPP	113.2	113.1	110.5	113.3	125.6	104.3	104.8	104.4	109.9	112.2	117.6	113.4	108.3	106.7	98.4	108.1	116.2	99.4	111.0
w/o AC	103.1	108.6	102.2	108.0	107.5	105.6	103.3	105.7	108.6	118.5	114.2	103.1	104.2	105.2	102.4	105.9	100.3	103.5	113.9
w/ DPC	101.5	106.5	101.9	105.8	99.8	101.8	102.1	100.8	100.8	107.2	113.5	100.4	103.0	110.5	102.1	107.2	98.0	104.4	103.5
w/o LRL	101.2	103.9	100.5	103.8	103.8	104.8	106.4	105.1	105.4	115.9	105.6	93.1	101.1	102.8	103.1	106.7	99.5	102.5	101.5
w/ GAP	101.1	98.6	98.7	98.9	97.1	105.8	107.5	105.7	107.8	111.8	108.9	97.1	103.7	101.7	100.5	105.6	105.8	100.2	102.2
Xception-41	100.0	100.0	100.0	100.0	100.0	100.0	100.0	100.0	100.0	100.0	100.0	100.0	100.0	100.0	100.0	100.0	100.0	100.0	100.0
w/o ASPP	105.1	98.5	107.5	98.5	112.2	102.4	103.5	102.4	105.3	109.8	108.9	110.2	110.2	102.3	100.2	98.8	112.4	98.2	116.9
w/o AC	98.5	98.3	99.5	100.4	102.6	99.1	102.0	99.3	101.6	104.0	105.6	104.7	108.2	106.8	100.5	100.0	96.6	99.6	107.5
w/ DPC	102.8	104.2	100.5	104.9	101.0	102.4	108.0	101.6	101.9	100.4	100.0	108.1	111.9	104.1	100.8	93.6	102.1	100.0	104.4
w/o LRL	98.2	103.6	100.9	103.7	103.9	94.9	97.7	92.3	90.1	94.0	99.2	103.9	107.7	107.6	97.2	96.9	100.0	95.9	108.0
w/ GAP	100.3	100.2	95.7	101.7	101.8	96.5	101.1	95.9	100.5	103.9	94.3	98.5	102.6	103.8	102.1	96.2	101.9	97.5	101.6
Xception-65	100.0	100.0	100.0	100.0	100.0	100.0	100.0	100.0	100.0	100.0	100.0	100.0	100.0	100.0	100.0	100.0	100.0	100.0	100.0
w/o ASPP	106.4	107.2	102.0	111.4	111.7	100.8	103.3	101.4	105.9	109.3	111.2	104.7	105.5	102.5	104.5	107.7	109.1	100.6	107.5
w/o AC	100.1	101.0	102.6	103.3	104.8	101.1	95.3	100.5	100.9	102.7	105.6	102.1	106.0	94.8	104.4	98.7	107.4	103.1	103.1
w/ DPC	104.0	109.8	105.1	111.6	108.9	107.2	106.5	108.3	109.3	97.9	109.9	126.3	101.4	101.7	102.4	107.4	111.0	102.5	107.1
w/o LRL	98.3	101.1	107.0	103.2	104.0	99.8	98.4	99.9	100.6	101.3	106.1	103.1	99.9	93.4	101.1	108.9	100.3	102.4	104.8
w/ GAP	100.0	99.1	98.5	101.0	102.5	95.5	94.6	95.2	97.8	101.5	101.9	106.6	96.5	99.9	100.6	102.6	112.4	104.2	106.3
Xception-71	100.0	100.0	100.0	100.0	100.0	100.0	100.0	100.0	100.0	100.0	100.0	100.0	100.0	100.0	100.0	100.0	100.0	100.0	100.0
w/o ASPP	109.6	103.6	101.1	105.2	115.1	95.7	95.6	96.5	102.4	110.9	114.6	106.0	108.3	100.5	101.6	102.9	116.1	97.9	105.9
w/o AC	105.3	107.6	100.4	105.7	100.9	108.4	105.8	110.2	114.3	114.0	101.4	107.4	102.0	99.1	100.9	100.8	108.2	98.2	99.7
w/ DPC	103.7	103.7	98.8	105.6	97.9	108.9	109.0	110.8	113.9	115.5	110.2	98.2	103.4	113.7	105.5	103.7	100.2	99.2	96.0
w/o LRL	99.8	94.0	102.8	95.4	98.7	101.1	101.7	101.5	99.9	100.5	111.0	98.7	105.4	106.9	102.4	103.6	99.3	98.5	98.7
w/ GAP	99.8	97.8	91.8	99.3	94.0	106.1	102.8	106.9	107.3	109.1	100.1	96.2	97.7	99.3	102.6	98.9	105.4	99.0	90.8

Table B.3: CD for corrupted variants of the validation set of the Cityscapes dataset for several network backbones of the DeepLabv3+ architecture and respective architectural ablations. Highest CD per corruption is bold.

Deeplab-v3+ Backbone	Blur					Noise					Digital				Weather				Geometric Distortion	
	Motion	Defocus	Frosted Glass	Gaussian	PSF	Gaussian	Impulse	Shot	Speckle	Intensity	Brightness	Contrast	Saturate	JPEG	Snow	Spatter	Fog	Frost		
MobileNet-V2	100.0	100.0	100.0	100.0	100.0	100.0	100.0	100.0	100.0	100.0	100.0	100.0	100.0	100.0	100.0	100.0	100.0	100.0	100.0	
	104.8	106.3	96.8	102.1	101.3	87.2	86.3	85.7	81.2	80.8	114.0	114.0	94.1	98.7	88.9	84.9	109.9	93.0	46.3	
	w/o AC	103.2	96.1	106.4	95.8	89.0	103.0	98.3	101.9	93.1	105.5	99.0	100.5	96.3	104.9	80.5	105.4	99.6	117.2	
	w/ DPC	119.9	127.8	104.3	121.3	152.5	103.8	102.6	103.4	100.2	97.9	130.9	130.5	104.7	106.0	105.9	87.1	112.5	105.1	143.2
	w/o LRL	115.5	118.1	100.0	113.8	141.6	105.4	105.4	104.8	92.8	97.9	108.5	109.2	98.1	100.0	104.1	95.5	106.5	103.0	155.2
	w/ GAP	103.5	90.4	105.0	85.8	100.6	95.8	93.0	92.6	81.9	86.1	96.7	95.2	91.1	102.0	100.5	84.7	106.6	107.3	81.9
ResNet-50	100.0	100.0	100.0	100.0	100.0	100.0	100.0	100.0	100.0	100.0	100.0	100.0	100.0	100.0	100.0	100.0	100.0	100.0	100.0	
	w/o ASPP	106.1	103.7	102.8	102.9	98.2	87.5	86.6	86.5	88.4	83.3	115.1	105.2	97.5	93.8	92.1	94.9	139.3	98.0	78.0
	w/o AC	106.7	114.5	97.5	115.9	126.3	104.9	100.7	106.5	111.0	110.0	103.9	112.5	105.0	98.4	102.6	101.7	116.3	103.9	128.5
	w/ DPC	110.3	111.1	102.1	110.2	154.5	94.5	92.8	95.2	96.3	98.3	121.6	106.6	100.5	105.5	101.5	102.8	99.8	105.1	118.1
	w/o LRL	98.2	106.0	99.5	106.5	106.5	96.7	95.5	96.8	96.5	89.5	105.4	109.8	100.3	95.8	98.7	99.0	98.3	101.4	108.8
	w/ GAP	109.7	104.3	104.7	101.3	73.1	101.4	99.0	100.7	99.4	91.9	102.5	114.9	100.3	98.1	102.3	104.5	106.9	104.9	113.4
ResNet-101	100.0	100.0	100.0	100.0	100.0	100.0	100.0	100.0	100.0	100.0	100.0	100.0	100.0	100.0	100.0	100.0	100.0	100.0	100.0	
	w/o ASPP	96.5	98.6	98.3	98.3	119.0	96.4	97.0	96.1	100.6	103.6	106.5	100.5	96.7	95.5	88.7	94.0	105.9	88.1	63.9
	w/o AC	99.3	111.4	99.2	110.4	125.1	105.5	102.3	105.5	110.1	126.1	124.6	100.1	103.0	104.7	101.1	105.8	94.3	102.4	138.4
	w/ DPC	103.0	113.2	103.1	112.2	92.1	102.3	102.7	101.0	101.0	111.4	130.4	100.4	104.7	116.3	102.7	112.6	95.5	106.1	112.9
	w/o LRL	99.5	105.5	98.9	105.4	120.0	105.7	107.9	106.1	107.1	124.1	109.5	83.7	100.3	102.9	103.3	110.0	96.3	102.4	98.4
	w/ GAP	103.8	98.2	98.5	98.9	74.0	108.3	110.6	108.3	112.8	119.8	121.7	95.1	106.8	103.4	101.0	110.8	112.9	100.7	112.2
Xception-41	100.0	100.0	100.0	100.0	100.0	100.0	100.0	100.0	100.0	100.0	100.0	100.0	100.0	100.0	100.0	100.0	100.0	100.0	100.0	
	w/o ASPP	97.7	86.9	104.9	86.8	133.6	99.4	100.9	99.1	101.9	109.2	106.3	109.9	109.9	97.7	96.4	90.5	114.4	93.4	146.1
	w/o AC	94.3	95.3	97.8	99.4	116.9	98.3	102.2	98.5	101.6	106.0	112.1	108.2	114.0	109.8	100.1	98.9	91.2	98.9	135.6
	w/ DPC	104.7	106.9	99.8	108.2	96.2	102.7	110.4	101.7	102.2	99.7	97.8	115.3	120.9	105.6	100.5	88.1	102.8	99.5	118.1
	w/o LRL	89.6	102.9	98.0	103.0	97.2	91.4	95.3	87.5	80.8	86.0	91.0	103.3	112.5	109.4	94.5	91.5	95.2	92.6	124.8
	w/ GAP	96.7	97.6	89.7	100.5	88.3	94.1	100.4	93.1	99.0	104.6	80.9	93.8	102.4	104.3	101.8	91.4	100.9	95.4	95.5
Xception-65	100.0	100.0	100.0	100.0	100.0	100.0	100.0	100.0	100.0	100.0	100.0	100.0	100.0	100.0	100.0	100.0	100.0	100.0	100.0	
	w/o ASPP	98.0	101.7	93.6	110.6	106.5	97.0	100.4	97.4	102.1	107.4	109.7	96.4	101.1	98.1	101.7	104.3	104.8	96.1	90.2
	w/o AC	95.0	98.1	101.8	103.1	121.2	100.2	92.7	99.3	99.3	102.2	109.3	100.5	107.7	90.7	104.7	94.9	113.0	103.0	101.7
	w/ DPC	105.0	117.0	106.5	120.8	181.5	108.5	107.4	110.2	112.8	94.2	121.2	152.0	100.0	100.9	102.1	110.6	122.2	102.2	121.3
	w/o LRL	90.4	98.3	109.8	102.7	108.8	98.6	96.8	98.5	98.8	99.7	110.2	102.5	97.5	88.8	100.1	113.1	95.5	101.9	109.2
	w/ GAP	99.7	97.8	97.0	102.0	132.6	93.9	92.8	93.4	96.4	102.4	104.8	113.8	94.1	99.7	100.7	104.4	130.2	105.7	129.1
Xception-71	100.0	100.0	100.0	100.0	100.0	100.0	100.0	100.0	100.0	100.0	100.0	100.0	100.0	100.0	100.0	100.0	100.0	100.0	100.0	
	w/o ASPP	91.2	81.3	84.3	85.5	49.1	86.9	87.3	87.3	91.1	102.4	99.6	88.8	99.0	88.4	94.2	88.3	107.3	89.1	60.7
	w/o AC	107.9	112.4	97.9	108.1	76.3	110.0	106.5	112.6	120.5	121.8	97.1	111.5	101.0	96.7	99.9	98.7	114.9	96.3	89.1
	w/ DPC	110.3	109.0	98.5	113.1	84.6	112.2	112.1	115.0	122.3	127.6	132.1	97.1	106.2	121.8	107.7	107.1	101.6	99.2	86.8
	w/o LRL	94.2	82.5	102.1	85.8	53.0	100.3	101.1	100.7	97.7	98.1	125.9	93.4	106.6	108.7	102.0	103.6	92.9	96.7	85.1
	w/ GAP	98.9	94.6	85.0	98.1	33.6	108.0	103.5	109.2	111.2	115.6	99.5	91.8	95.8	98.8	103.3	97.8	112.7	98.5	64.1

	Blur					Noise					Digital				Weather				Geometric Distortion
Deeplab-v3+ Backbone	Clean	Motion	Defocus	Frosted Glass	Gaussian	Gaussian	Impulse	Shot	Speckle	Intensity	Brightness	Contrast	Saturate	JPEG	Snow	Spatter	Fog	Frost	
ResNet-50	69.6	38.7	43.5	31.1	45.5	43.2	40.7	44.2	50.9	59.8	63.5	50.3	63.8	58.2	31.3	47.0	56.9	39.8	67.2
w/o ASPP	57.6	28.8	28.8	21.9	31.5	31.7	29.2	32.3	38.4	45.9	49.8	36.0	51.1	45.0	23.1	37.6	42.0	26.7	56.3
w/o AC	68.9	39.3	41.6	29.0	43.6	43.6	42.0	44.1	50.8	59.3	62.7	48.9	62.9	56.9	31.2	46.4	55.9	38.3	65.9
w/ DPC	68.0	38.6	40.6	29.7	42.5	44.0	42.2	45.2	51.6	59.8	61.5	48.9	62.6	56.5	30.4	46.8	56.0	37.9	64.9
w/o LRL	69.0	40.0	41.2	30.1	43.0	43.5	41.9	44.3	50.8	59.7	62.4	48.5	62.5	57.2	30.4	46.6	55.8	39.1	65.5
w/ GAP	71.5	41.6	42.9	33.0	45.9	45.6	45.3	46.4	53.7	63.4	65.7	52.1	66.1	59.5	33.6	50.0	60.3	43.8	67.6
ResNet-101	70.3	45.8	45.6	33.2	46.6	49.4	48.3	50.1	55.4	61.3	64.5	50.6	65.3	59.7	31.4	50.4	57.6	41.2	67.6
w/o ASPP	60.5	36.4	34.2	25.1	36.3	36.4	34.1	37.1	43.0	50.5	53.6	39.2	54.1	49.8	24.5	41.9	45.5	29.6	59.8
w/o AC	70.2	46.8	45.8	33.5	46.3	46.0	45.2	46.6	52.9	60.5	64.4	50.5	64.5	59.6	32.3	51.0	57.9	40.4	66.8
w/ DPC	69.5	44.5	44.8	32.3	46.2	48.4	45.0	49.4	54.8	61.5	63.5	51.3	64.0	59.4	32.3	49.9	58.3	40.5	65.7
w/o LRL	69.6	44.2	44.8	33.5	45.8	47.4	45.2	48.5	53.8	61.3	64.1	50.7	64.6	58.4	32.2	50.6	57.5	40.4	65.9
w/ GAP	72.5	46.7	46.3	36.5	47.6	50.5	48.5	51.3	56.6	64.3	66.7	53.6	66.0	61.1	36.4	52.6	61.7	44.7	68.4
Xception-41	75.5	52.9	54.7	35.5	53.9	55.8	53.3	56.7	62.8	67.6	70.8	51.9	70.9	64.6	42.5	59.0	63.1	48.4	73.0
w/o ASPP	66.9	45.9	45.3	30.4	45.6	47.2	45.5	48.0	52.9	58.5	61.0	43.1	61.5	56.0	34.6	50.6	53.1	39.3	65.4
w/o AC	75.0	53.2	54.9	36.5	54.9	54.1	52.6	55.5	61.4	67.1	69.7	50.5	70.5	64.5	40.9	60.1	62.3	47.0	71.8
w/ DPC	75.3	51.6	54.8	37.5	54.3	56.8	55.1	58.1	63.0	67.8	70.0	50.8	70.7	65.5	40.6	58.1	61.9	47.7	72.0
w/o LRL	76.1	52.9	56.7	36.7	55.8	56.7	56.6	58.3	63.9	68.8	70.9	53.8	71.9	65.1	41.4	59.1	63.3	48.4	72.9
w/ GAP	76.5	55.0	55.2	36.3	55.0	55.3	55.7	56.6	62.7	68.8	71.1	52.8	71.5	66.1	43.3	61.4	63.7	48.9	72.3
Xception-65	76.5	53.5	58.3	37.7	57.2	56.6	54.7	57.4	62.5	69.3	71.8	55.9	72.1	66.7	40.2	58.5	64.0	47.5	73.6
w/o ASPP	70.6	47.5	47.8	29.1	48.6	45.4	44.2	45.6	51.8	62.4	64.7	48.1	64.6	58.3	35.7	52.6	56.4	39.4	68.7
w/o AC	76.4	57.6	57.3	38.4	56.9	56.5	54.5	57.0	62.2	69.6	71.4	55.0	72.3	66.3	42.5	60.4	63.6	46.4	73.6
w/ DPC	76.1	53.7	55.0	34.6	55.0	54.8	54.0	56.0	61.6	68.9	70.9	54.0	71.1	66.0	40.9	58.3	61.9	46.5	73.4
w/o LRL	76.2	55.2	55.1	36.6	55.6	56.5	55.4	56.8	61.8	68.9	71.1	56.1	71.1	64.3	40.3	58.4	64.2	46.1	73.0
w/ GAP	77.5	56.8	59.8	41.8	59.1	57.9	57.6	57.6	62.6	71.0	73.1	57.4	73.0	67.3	42.8	61.1	65.3	49.7	73.2
Xception-71	76.7	56.5	59.1	40.2	59.5	56.6	57.8	57.6	63.2	69.9	72.1	57.1	72.6	68.1	43.9	60.9	66.1	50.9	73.6
w/o ASPP	70.5	48.3	49.2	33.3	50.1	47.5	47.1	48.2	54.6	62.7	65.1	48.8	65.6	60.2	37.0	53.4	57.3	44.1	69.3
w/o AC	75.7	55.9	58.8	41.8	59.0	57.1	58.2	57.3	62.6	69.5	71.0	56.9	71.4	67.6	41.9	60.9	64.1	48.2	73.0
w/ DPC	76.8	53.5	54.6	35.8	55.4	55.5	55.6	54.7	60.5	69.0	71.4	54.0	71.0	66.3	42.5	58.3	63.3	49.7	73.3
w/o LRL	76.3	56.4	56.4	40.5	55.9	59.9	59.3	60.2	64.6	71.1	72.1	53.0	72.3	67.7	43.8	59.3	64.1	50.8	73.2
w/ GAP	77.7	57.8	58.7	38.3	59.1	58.8	55.2	58.4	63.7	71.9	73.8	60.4	73.9	69.2	46.9	61.6	67.9	53.5	73.5

Table B.5: Mean IoU for clean and corrupted variants of the validation set of PASCAL VOC 2012 for several network backbones of the Deeplabv3+ architecture and respective architectural ablations. Every mIoU is averaged over all available severity levels, except for corruptions of category noise where only the first three severity levels are considered. The standard deviation for image corruptions of category noise is 0.3 or less. Highest mIoU per corruption is bold.

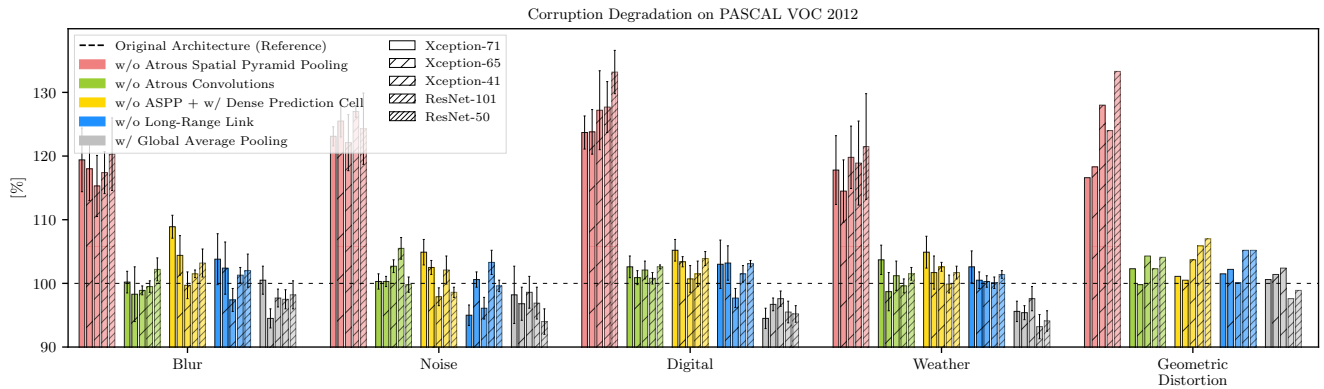


Figure B.10: CD evaluated on PASCAL VOC 2012 for the proposed ablated variants of the Deeplabv3+ architecture w.r.t. image corruptions, employing five different network backbones. Each bar except for geometric distortion is averaged within a corruption category (error bars indicate the standard deviation). Bars above 100 % represent a decrease in performance compared to the respective reference architecture. Each ablated architecture is re-trained on the original training dataset. Removing ASPP reduces the model performance significantly. AC and LRL decrease robustness against corruptions of category *digital* slightly. Xception-71 is vulnerable against many corruptions when DPC is used. GAP increases performance against many corruptions. Each backbone performs further best on clean data when GAP is used. Best viewed in color.

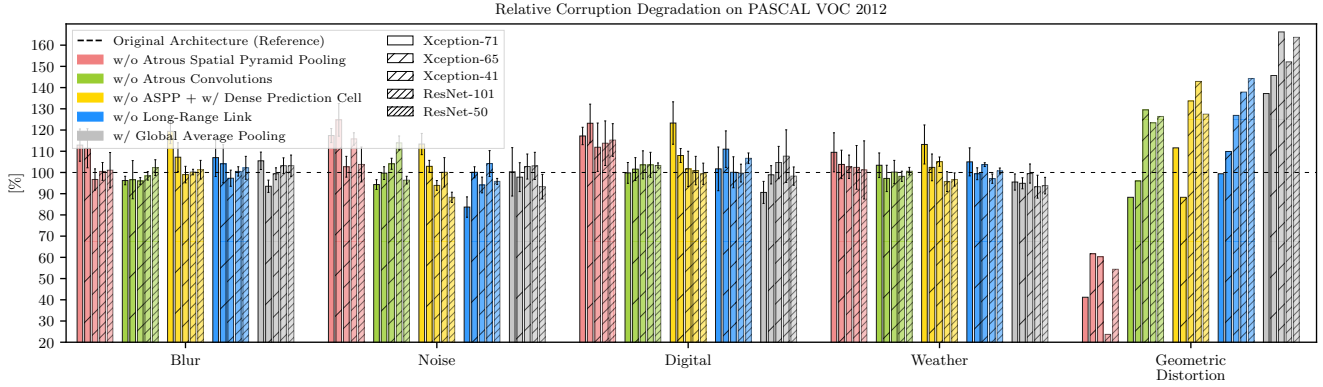


Figure B.11: Relative CD evaluated on PASCAL VOC 2012 for the proposed ablated variants of the DeepLabv3+ architecture w.r.t. image corruptions, employing five different network backbones. Each bar except for geometric distortion is averaged within a corruption category (error bars indicate the standard deviation). Bars above 100 % represent a relative decrease in performance compared to the respective reference architecture. Each ablated architecture is re-trained on the original training dataset. Removing ASPP decreases performance oftentimes significantly. The low rCD for geometric distortion indicates that the relative decrease of performance for this ablated variant is low. AC aids the robustness against geometric distortion for several backbones. The harming effect of DPC with respect to image corruptions is especially pronounced for Xception-71. The rCD of LRL is large against geometric distortion for ResNet-50. The rCD of GAP has, oftentimes, a contrary tendency as the CD. Best viewed in color.

Deeplab-v3+ Backbone	Blur				Noise					Digital				Weather				Geometric Distortion
	Motion	Defocus	Frosted Glass	Gaussian	Gaussian	Impulse	Shot	Speckle	Intensity	Brightness	Contrast	Saturate	JPEG	Snow	Spatter	Fog	Frost	
ResNet-50	100.0	100.0	100.0	100.0	100.0	100.0	100.0	100.0	100.0	100.0	100.0	100.0	100.0	100.0	100.0	100.0	100.0	100.0
w/o ASPP	116.1	126.1	113.3	125.7	120.3	119.4	121.4	125.6	134.7	137.7	128.7	135.0	131.4	111.9	117.8	134.5	121.7	133.3
w/o AC	99.1	103.4	103.0	103.5	99.3	97.9	100.2	100.4	101.3	102.3	102.6	102.4	103.1	100.0	101.1	102.2	102.6	104.1
w/ DPC	100.2	105.2	101.9	105.5	98.6	97.6	98.2	98.6	100.1	105.5	102.6	103.2	104.0	101.3	100.5	101.9	103.3	107.0
w/o LRL	98.0	104.1	101.5	104.6	99.4	98.0	99.9	100.3	100.3	103.0	103.6	103.4	102.4	101.2	100.9	102.4	101.2	105.2
w/ GAP	95.4	101.1	97.2	99.4	95.9	92.3	96.2	94.3	91.2	94.0	96.3	93.7	96.7	96.6	94.4	92.1	93.5	98.9
ResNet-101	100.0	100.0	100.0	100.0	100.0	100.0	100.0	100.0	100.0	100.0	100.0	100.0	100.0	100.0	100.0	100.0	100.0	100.0
w/o ASPP	117.2	120.9	112.2	119.4	125.7	127.4	126.1	127.8	127.9	130.9	123.0	132.3	124.5	110.1	117.1	128.5	119.8	124.0
w/o AC	98.1	99.6	99.5	100.7	106.7	106.0	107.0	105.7	102.1	100.5	100.1	102.3	100.4	98.7	98.8	99.3	101.4	102.3
w/ DPC	102.3	101.4	101.4	100.8	102.0	106.2	101.5	101.4	99.5	103.0	98.6	103.6	100.9	98.7	101.2	98.3	101.3	105.9
w/o LRL	102.9	101.4	99.6	101.5	103.9	105.9	103.3	103.5	100.0	101.2	99.7	102.0	103.3	99.0	99.6	100.2	101.5	105.2
w/ GAP	98.3	98.6	95.0	98.2	97.8	99.5	97.7	97.2	92.2	93.8	93.9	97.8	96.6	92.8	95.6	90.4	94.0	97.6
Xception-41	100.0	100.0	100.0	100.0	100.0	100.0	100.0	100.0	100.0	100.0	100.0	100.0	100.0	100.0	100.0	100.0	100.0	100.0
w/o ASPP	114.8	120.8	107.9	117.9	119.3	116.6	120.1	126.5	127.9	133.7	118.3	132.3	124.4	113.6	120.6	127.2	117.6	128.0
w/o AC	99.4	99.7	98.5	97.8	103.9	101.5	103.0	103.6	101.6	103.7	103.0	101.4	100.2	102.7	97.3	102.2	102.7	104.3
w/ DPC	102.9	99.8	97.0	99.1	97.8	96.1	96.8	99.4	99.4	102.6	102.3	100.5	97.4	103.2	102.3	103.2	101.5	103.7
w/o LRL	100.0	95.6	98.2	95.8	97.9	92.9	96.5	97.0	96.1	99.6	96.0	96.6	98.6	101.8	99.8	99.5	100.0	100.1
w/ GAP	95.5	99.0	98.8	97.5	101.2	94.9	100.3	100.3	96.4	99.0	98.1	97.8	95.7	98.6	94.3	98.4	99.0	102.4
Xception-65	100.0	100.0	100.0	100.0	100.0	100.0	100.0	100.0	100.0	100.0	100.0	100.0	100.0	100.0	100.0	100.0	100.0	100.0
w/o ASPP	112.8	125.2	113.9	120.2	125.9	123.1	127.5	128.7	122.3	125.3	117.7	126.7	125.3	107.4	114.0	121.1	115.4	118.3
w/o AC	91.1	102.5	98.9	100.7	100.3	100.5	100.9	101.0	98.8	101.3	102.2	99.1	101.2	96.2	95.4	101.2	102.1	99.8
w/ DPC	99.5	108.0	104.9	105.3	104.1	101.5	103.2	102.6	101.2	103.4	104.4	103.5	102.3	98.8	100.3	105.8	101.9	100.5
w/o LRL	96.3	107.7	101.8	103.8	100.3	98.4	101.2	101.9	101.2	102.6	99.7	103.4	107.1	99.7	100.3	99.4	102.7	102.2
w/ GAP	92.8	96.4	93.4	95.6	97.0	93.6	99.4	99.8	94.3	95.3	96.6	96.7	98.2	95.6	93.6	96.5	95.7	101.4
Xception-71	100.0	100.0	100.0	100.0	100.0	100.0	100.0	100.0	100.0	100.0	100.0	100.0	100.0	100.0	100.0	100.0	100.0	100.0
w/o ASPP	118.9	124.3	111.5	123.0	121.0	125.2	122.0	123.4	123.8	125.0	119.2	125.6	124.9	112.3	119.1	126.0	113.9	116.6
w/o AC	101.3	100.9	97.3	101.2	98.8	99.0	100.7	101.8	101.4	103.9	100.4	104.4	101.5	103.5	100.1	105.9	105.4	102.3
w/ DPC	107.0	111.1	107.4	110.1	102.5	105.1	106.7	107.5	102.9	102.4	107.1	105.8	105.5	102.5	106.7	108.1	102.5	101.1
w/o LRL	100.2	106.7	99.5	108.7	92.4	96.5	93.9	96.3	95.9	99.9	109.4	101.2	101.2	100.2	104.0	105.8	100.2	101.5
w/ GAP	97.1	101.1	103.2	100.8	94.8	106.1	98.2	98.7	93.2	93.9	92.3	95.2	96.5	94.7	98.3	94.7	94.7	100.6

Table B.6: Mean CD for corrupted variants of the validation set of PASCAL VOC 2012 for several network backbones of the DeepLabv3+ architecture and respective architectural ablations. Highest CD per corruption is bold.

Deeplab-v3+ Backbone	Blur				Noise					Digital				Weather				Geometric Distortion
	Motion	Defocus	Frosted Glass	Gaussian	Gaussian	Impulse	Shot	Speckle	Intensity	Brightness	Contrast	Saturate	JPEG	Snow	Spatter	Fog	Frost	
ResNet-50	100.0	100.0	100.0	100.0	100.0	100.0	100.0	100.0	100.0	100.0	100.0	100.0	100.0	100.0	100.0	100.0	100.0	100.0
w/o ASPP	93.1	110.4	92.6	108.2	98.3	98.3	99.8	103.0	119.8	128.6	111.6	111.1	109.9	90.0	88.7	122.6	103.6	100.0
w/o AC	95.9	104.7	103.6	105.0	95.8	93.2	97.7	97.2	98.2	102.1	103.2	102.8	105.2	98.2	99.5	102.0	102.8	126.4
w/ DPC	95.1	105.0	99.2	105.7	90.7	89.4	89.7	87.7	83.8	106.3	98.4	92.2	100.5	98.1	94.0	93.6	101.2	127.5
w/o LRL	93.9	106.4	100.9	107.7	96.3	93.7	97.1	97.4	94.7	107.4	106.0	110.1	103.1	100.5	99.1	103.0	100.2	144.3
w/ GAP	96.9	109.5	99.8	106.4	98.2	90.8	99.1	95.2	83.2	95.3	100.1	93.5	104.5	98.7	95.1	88.1	93.2	163.7
ResNet-101	100.0	100.0	100.0	100.0	100.0	100.0	100.0	100.0	100.0	100.0	100.0	100.0	100.0	100.0	100.0	100.0	100.0	100.0
w/o ASPP	98.0	106.3	95.4	102.3	115.3	119.7	115.8	117.3	111.0	119.4	107.8	127.7	100.5	92.6	93.3	117.7	106.2	23.7
w/o AC	95.4	98.5	98.7	101.1	115.7	113.4	116.6	116.1	107.8	100.9	99.5	113.7	100.1	97.4	96.4	96.8	102.4	123.4
w/ DPC	102.0	99.9	100.4	98.5	101.0	111.1	99.9	99.1	89.4	105.3	92.7	109.4	96.1	95.8	99.1	88.1	99.9	142.9
w/o LRL	103.7	100.3	97.4	100.6	106.3	110.9	105.0	106.1	92.7	96.1	95.9	100.7	106.3	96.5	95.6	95.3	100.8	137.9
w/ GAP	105.1	105.7	96.8	105.1	105.0	108.7	105.2	106.3	90.6	99.6	95.7	127.9	107.4	92.9	99.9	85.0	95.4	152.1
Xception-41	100.0	100.0	100.0	100.0	100.0	100.0	100.0	100.0	100.0	100.0	100.0	100.0	100.0	100.0	100.0	100.0	100.0	100.0
w/o ASPP	93.0	104.0	91.3	98.6	99.9	96.4	100.7	110.4	106.0	127.2	101.1	118.5	100.7	97.8	99.3	111.8	102.0	60.3
w/o AC	96.9	97.3	96.6	93.4	106.5	101.1	104.5	107.1	101.1	113.9	104.2	99.4	96.7	103.4	90.6	103.1	103.6	129.5
w/ DPC	105.3	98.9	94.8	97.2	94.2	91.0	91.7	97.0	95.5	112.9	103.9	99.9	89.9	105.2	104.7	108.4	102.2	133.7
w/o LRL	102.9	93.5	98.8	94.0	98.5	87.9	95.4	96.2	92.4	111.5	94.6	92.8	101.3	105.1	103.5	103.7	102.5	126.9
w/ GAP	95.0	102.8	100.6	99.3	107.8	93.7	106.0	108.7	97.9	115.4	100.4	107.8	95.3	100.6	92.0	103.5	101.9	166.2
Xception-65	100.0	100.0	100.0	100.0	100.0	100.0	100.0	100.0	100.0	100.0	100.0	100.0	100.0	100.0	100.0	100.0	100.0	100.0
w/o ASPP	100.1	124.9	106.9	113.8	126.4	120.7	130.2	134.3	112.4	124.8	109.0	133.9	125.0	95.8	99.3	113.0	107.3	61.7
w/o AC	81.7	105.2	98.1	101.3	100.4	100.6	101.7	102.0	93.8	106.5	104.3	92.5	103.3	93.5	89.0	103.0	103.5	96.0
w/ DPC	96.9	115.7	106.7	109.3	106.5	101.1	104.7	103.5	98.4	110.5	107.2	111.3	102.9	96.7	98.1	112.9	101.8	88.3
w/o LRL	91.2	116.1	102.2	106.9	99.3	95.5	101.3	103.1	101.1	109.5	98.0	115.1	121.4	98.7	99.1	96.0	103.8	109.9
w/ GAP	89.7	97.1	91.9	95.4	98.5	91.1	103.8	106.6	89.3	92.7	97.5	101.6	103.9	95.5	90.6	97.8	95.6	145.7
Xception-71	100.0	100.0	100.0	100.0	100.0	100.0	100.0	100.0	100.0	100.0	100.0	100.0	100.0	100.0	100.0	100.0	100.0	100.0
w/o ASPP	110.1	121.4	101.9	118.3	114.5	123.5	116.5	118.0	114.6	117.1	110.6	120.5	120.6	102.2	108.2	124.9	102.6	41.2
w/o AC	98.1	96.6	92.9	97.3	92.7	92.7	96.6	97.7	91.9	102.8	96.0	106.3	94.3	103.1	94.3	109.8	106.6	88.3
w/ DPC	115.3	126.1	112.2	124.2	105.6	111.6	115.1	120.9	113.5	115.8	115.9	140.2	121.2	104.4	116.9	126.6	104.9	111.6
w/o LRL	98.4	113.3	98.1	118.1	81.6	90.0	84.3	86.8	75.8	90.7	118.6	97.8	99.8	99.0	107.4	114.8	98.7	99.4
w/ GAP	98.5	108.2	107.9	107.5	93.7	118.8	101.0	103.7	84.2	84.3	88.1	91.6	98.3	93.9	102.0	92.3	93.7	137.2

Table B.7: Relative CD for corrupted variants of the validation set of PASCAL VOC 2012 for several network backbones of the DeepLabv3+ architecture and respective architectural ablations. Highest rCD per corruption is bold.

Deeplab-v3+ Backbone	Blur					Noise					Digital				Weather				Geometric Distortion
	Clean	Motion	Defocus	Frosted Glass	Gaussian	Gaussian	Impulse	Shot	Speckle	Intensity	Brightness	Contrast	Saturate	JPEG	Snow	Spatter	Fog	Frost	
MobileNet-V2	33.1	16.1	16.6	14.9	16.5	12.1	11.5	12.4	17.0	24.7	27.2	14.8	26.5	25.1	7.8	18.5	20.1	10.7	28.3
w/o ASPP	27.3	12.2	11.3	10.5	11.6	9.6	9.6	9.9	13.3	19.0	22.1	10.8	20.8	19.5	5.7	15.6	14.5	7.8	22.9
w/o AC	32.1	15.2	15.9	14.2	15.7	11.2	11.5	11.4	15.6	23.0	27.1	13.7	25.1	25.1	7.6	18.8	19.2	10.7	27.9
w/ DPC	34.7	17.3	18.9	15.6	18.0	13.9	13.7	13.8	18.4	25.8	28.9	15.8	27.8	26.2	8.6	20.8	21.5	11.6	29.4
w/o LRL	32.2	15.7	16.5	14.3	16.3	12.9	11.6	13.2	17.3	24.4	26.7	14.2	25.1	24.6	7.5	18.9	19.7	10.7	27.6
w/ GAP	33.9	17.2	17.9	15.1	17.2	12.5	12.8	12.8	16.8	25.3	28.7	15.0	27.4	26.6	8.7	20.9	20.8	11.7	29.1
ResNet-50	37.4	18.0	19.7	16.9	19.2	14.1	12.8	14.4	19.4	28.5	31.1	18.0	30.1	29.5	8.8	21.5	23.9	13.6	32.9
w/o ASPP	29.7	13.5	13.8	11.6	13.5	11.1	10.1	11.6	15.5	21.6	24.8	13.3	23.4	22.7	6.7	17.0	17.6	9.9	25.5
w/o AC	36.5	18.2	19.3	16.6	18.7	13.7	11.8	13.8	18.8	27.5	30.2	17.3	29.1	28.7	7.9	20.4	23.3	12.8	31.3
w/ DPC	37.9	18.9	20.3	17.5	19.8	13.4	12.2	13.7	19.2	29.0	31.6	18.9	30.3	30.1	8.6	20.9	24.5	13.6	33.0
w/o LRL	36.6	18.3	19.8	16.1	18.8	13.6	12.2	13.8	18.9	27.4	31.0	19.1	30.1	29.3	8.1	21.2	24.3	13.4	32.0
w/ GAP	38.2	19.3	21.1	17.2	19.9	15.5	12.8	15.8	21.3	30.4	32.9	19.5	31.7	30.8	9.9	23.2	25.8	14.9	33.0
ResNet-101	38.1	19.1	20.6	17.3	19.8	15.4	14.6	15.7	20.7	28.8	31.6	19.7	31.2	31.4	10.2	22.9	25.6	14.0	32.8
w/o ASPP	30.7	14.3	14.1	12.8	14.2	13.3	11.8	13.7	17.7	23.4	25.9	14.4	24.7	24.1	7.3	18.5	18.8	10.7	26.2
w/o AC	37.3	18.3	19.9	16.9	19.0	14.4	14.4	14.7	19.4	27.5	31.4	18.1	30.1	30.5	9.4	22.9	24.6	13.6	32.2
w/ DPC	37.6	19.6	21.0	17.7	20.0	15.9	15.1	16.4	21.6	28.7	32.1	19.5	31.5	31.2	9.7	23.3	25.4	14.0	32.6
w/o LRL	37.5	18.9	20.5	17.7	19.9	16.5	14.6	16.8	21.7	29.0	31.6	19.8	30.7	30.1	9.8	22.2	25.9	14.0	32.2
w/ GAP	39.3	20.2	21.7	17.9	20.6	15.9	14.2	16.1	21.4	29.9	33.2	20.4	32.8	32.8	10.8	23.3	27.0	15.6	34.2
Xception-41	39.7	22.1	22.7	17.4	20.8	20.8	18.1	20.5	24.8	33.7	34.2	20.9	32.5	32.6	13.0	25.0	28.4	17.0	34.4
w/o ASPP	35.4	19.4	20.0	15.3	18.4	18.2	16.3	17.9	21.7	29.2	30.3	17.7	28.5	28.3	11.2	22.7	23.5	14.4	31.3
w/o AC	38.4	21.8	22.2	17.7	20.6	21.8	18.3	21.1	25.0	32.9	33.4	20.0	31.7	32.0	12.2	24.8	26.4	15.9	33.0
w/ DPC	40.2	21.9	22.5	17.4	20.8	20.2	17.5	19.6	23.9	33.3	34.8	20.3	32.6	32.9	13.8	25.6	26.9	17.4	34.5
w/o LRL	39.1	21.4	22.6	17.2	20.6	20.8	17.6	20.5	25.0	32.6	34.1	21.1	32.1	32.2	13.8	25.5	27.1	16.9	34.2
w/ GAP	39.0	22.7	22.9	17.5	21.0	21.9	18.5	21.6	25.4	33.1	34.1	21.6	32.3	32.6	14.3	25.8	28.9	17.7	34.1
Xception-65	41.4	23.4	25.2	18.9	22.7	23.2	19.8	22.9	27.1	35.4	36.1	23.5	34.8	34.2	14.8	27.7	30.0	18.4	35.6
w/o ASPP	40.2	21.4	23.3	18.1	21.6	20.4	16.7	20.1	24.7	33.0	34.1	21.4	32.6	31.4	12.1	25.3	27.4	15.6	35.1
w/o AC	40.0	22.7	24.4	18.6	22.1	23.6	20.9	22.8	26.4	34.6	35.1	23.4	33.9	33.3	13.9	27.2	29.1	17.8	35.0
w/ DPC	40.9	23.7	24.9	18.4	22.8	23.0	18.8	22.9	27.0	35.6	35.7	23.0	34.1	33.9	14.6	28.0	29.5	17.9	35.7
w/o LRL	41.0	23.2	25.0	18.6	22.7	24.2	19.8	23.9	27.6	35.6	35.7	23.5	34.1	33.8	14.9	27.5	29.3	19.0	36.1
w/ GAP	41.7	23.9	25.6	19.2	23.4	24.7	20.8	24.2	28.1	36.2	36.1	23.8	35.0	34.1	15.4	28.2	30.5	20.1	36.0
Xception-71	42.4	24.4	26.4	19.5	23.9	24.0	20.3	23.3	27.5	36.8	37.2	25.3	35.7	34.7	16.1	29.4	31.3	19.8	37.1
w/o ASPP	40.6	21.9	24.2	17.5	21.9	20.8	16.6	20.0	24.2	34.0	34.8	22.5	33.1	32.4	12.9	26.3	28.9	16.5	35.2
w/o AC	41.8	24.3	25.4	19.6	23.6	24.0	19.9	22.9	26.2	35.7	36.1	23.2	34.8	33.7	15.7	28.3	29.9	19.7	35.8
w/ DPC	42.5	23.3	25.9	18.4	23.1	23.4	18.9	22.4	26.5	36.3	36.5	24.1	34.9	34.2	15.8	28.3	30.6	18.6	36.3
w/o LRL	42.2	22.9	25.9	18.7	23.5	21.7	18.7	21.1	25.4	35.5	36.3	24.3	34.5	34.0	15.1	28.6	30.6	19.7	36.4
w/ GAP	42.0	24.0	26.6	19.1	24.0	23.6	19.8	22.8	26.7	35.9	37.0	25.0	35.2	34.6	16.7	29.3	31.6	20.9	36.3

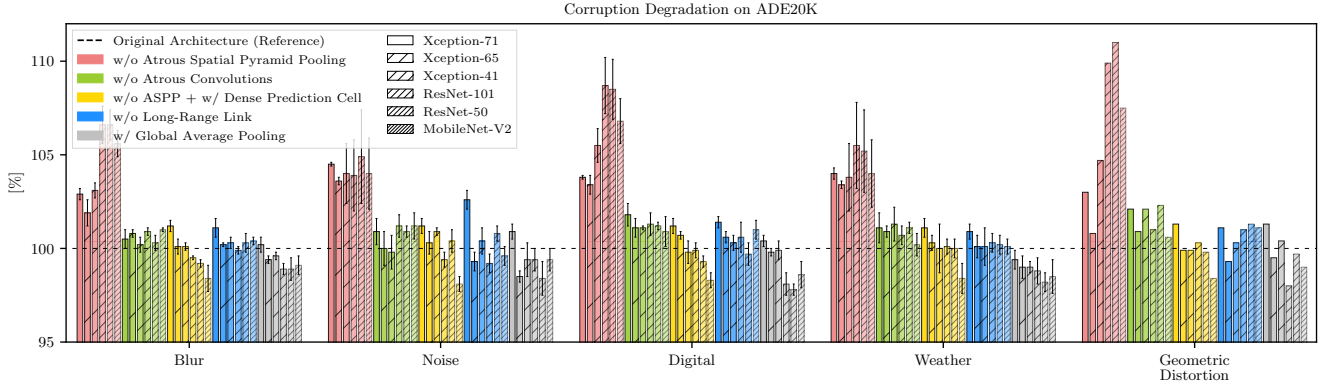


Figure B.12: CD evaluated on ADE20K for the proposed ablated variants of the DeepLabv3+ architecture w.r.t. image corruptions, employing six different network backbones. Each bar except for geometric distortion is averaged within a corruption category (error bars indicate the standard deviation). Bars above 100 % represent a relative decrease in performance compared to the respective reference architecture. Each ablated architecture is re-trained on the original training dataset. Removing ASPP decreases performance oftentimes. AC increase performance slightly against most corruptions. DPC and LRL hamper the performance for Xception-71 w.r.t. several image corruptions. GAP increases the robustness for most backbones against many image corruptions. Best viewed in color.

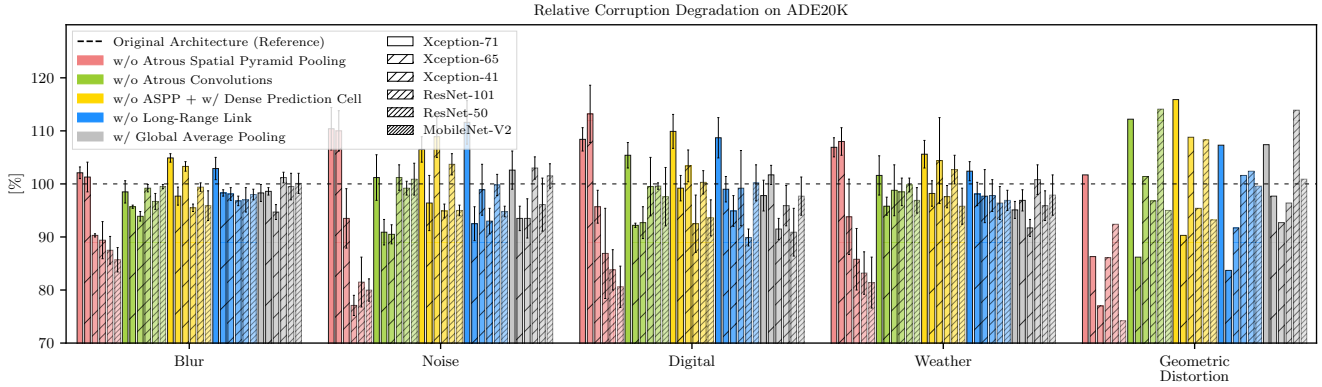


Figure B.13: Relative CD evaluated on ADE20K for the proposed ablated variants of the DeepLabv3+ architecture w.r.t. image corruptions, employing six different network backbones. Bars above 100 % represent a relative decrease in performance compared to the respective reference architecture. Each bar except for geometric distortion is averaged within a corruption category (error bars indicate the standard deviation). Each ablated architecture is re-trained on the original training dataset. Removing ASPP decreases performance oftentimes significantly. The low rCD for geometric distortion indicates that the relative decrease of performance for this ablated variant is low (except for Xception-71). The rCD of DPC and LRL are oftentimes highest for Xception-71. GAP increases the robustness for most backbones against many image corruptions. Best viewed in color.

Deeplab-v3+ Backbone	Blur				Noise					Digital				Weather				Geometric Distortion
	Motion	Defocus	Frosted Glass	Gaussian	Gaussian	Impulse	Shot	Speckle	Intensity	Brightness	Contrast	Saturate	JPEG	Snow	Spatter	Fog	Frost	
MobileNet-V2	100.0	100.0	100.0	100.0	100.0	100.0	100.0	100.0	100.0	100.0	100.0	100.0	100.0	100.0	100.0	100.0	100.0	100.0
w/o ASPP	104.7	106.4	105.2	105.9	102.9	102.1	102.8	104.5	107.5	107.0	104.8	107.8	107.5	102.3	103.6	107.1	103.3	107.5
w/o AC	101.1	100.9	100.8	101.0	101.1	100.0	101.1	101.7	102.1	100.1	101.3	102.0	100.0	100.2	99.6	101.1	100.0	100.6
w/ DPC	98.7	97.3	99.2	98.3	98.0	97.5	98.4	98.3	98.5	97.7	98.8	98.3	98.5	99.2	97.2	98.2	99.0	98.4
w/o LRL	100.6	100.1	100.8	100.3	99.1	99.8	99.1	99.6	100.3	100.8	100.8	102.0	100.7	100.4	99.5	100.6	100.0	101.1
w/ GAP	98.8	98.5	99.8	99.3	99.6	98.5	99.5	100.2	99.1	98.0	99.8	98.8	98.0	99.0	97.0	99.2	98.9	99.0
ResNet-50	100.0	100.0	100.0	100.0	100.0	100.0	100.0	100.0	100.0	100.0	100.0	100.0	100.0	100.0	100.0	100.0	100.0	100.0
w/o ASPP	105.4	107.4	106.4	107.1	103.5	103.1	103.3	104.8	109.7	109.2	105.8	109.5	109.6	102.2	105.8	108.3	104.3	111.0
w/o AC	99.7	100.6	100.5	100.6	100.5	101.1	100.8	100.6	101.4	101.3	100.9	101.4	101.2	101.0	101.5	100.8	100.9	102.3
w/ DPC	98.9	99.3	99.3	99.4	100.8	100.7	100.9	100.2	99.3	99.3	98.9	99.7	99.2	100.1	100.8	99.2	100.0	99.8
w/o LRL	99.6	99.9	101.0	100.6	100.6	100.7	100.7	100.5	101.6	100.1	98.7	99.9	100.3	100.7	100.4	99.5	100.3	101.3
w/ GAP	98.4	98.3	99.7	99.2	98.4	100.0	98.4	97.7	97.4	97.4	98.1	97.7	98.1	98.7	97.9	97.5	98.5	99.7
ResNet-101	100.0	100.0	100.0	100.0	100.0	100.0	100.0	100.0	100.0	100.0	100.0	100.0	100.0	100.0	100.0	100.0	100.0	100.0
w/o ASPP	105.9	108.1	105.5	107.0	102.5	103.2	102.3	103.8	107.5	108.4	106.5	109.4	110.6	103.2	105.7	109.2	103.9	109.9
w/o AC	101.0	100.8	100.5	101.0	101.2	100.2	101.2	101.6	101.8	100.3	101.9	101.5	101.3	100.9	100.0	101.4	100.5	101.0
w/ DPC	99.3	99.4	99.6	99.7	99.4	99.3	99.1	98.9	100.1	99.3	100.3	99.6	100.4	100.6	99.5	100.3	100.1	100.3
w/o LRL	100.2	100.1	99.6	99.9	98.7	100.0	98.7	98.8	99.6	100.0	99.9	100.7	101.9	100.5	100.9	99.6	100.0	101.0
w/ GAP	98.7	98.6	99.3	98.9	99.5	100.4	99.5	99.2	98.3	97.6	99.1	97.6	97.9	99.4	99.5	98.1	98.1	98.0
Xception-41	100.0	100.0	100.0	100.0	100.0	100.0	100.0	100.0	100.0	100.0	100.0	100.0	100.0	100.0	100.0	100.0	100.0	100.0
w/o ASPP	103.4	103.4	102.5	103.0	103.4	102.3	103.3	104.1	106.9	105.9	104.0	105.9	106.4	102.1	103.1	106.9	103.1	104.7
w/o AC	100.3	100.6	99.6	100.3	98.7	99.8	99.2	99.8	101.3	101.2	101.1	101.1	100.9	100.9	100.3	102.8	101.2	102.1
w/ DPC	100.3	100.2	99.9	100.0	100.8	100.8	101.2	101.2	100.7	99.1	100.8	99.8	99.6	99.1	99.3	102.2	99.4	99.9
w/o LRL	100.8	100.1	100.2	100.2	100.0	100.7	100.0	99.7	101.7	100.1	99.8	100.6	100.6	99.1	99.4	101.8	100.0	100.3
w/ GAP	99.2	99.6	99.9	99.7	98.6	99.5	98.5	99.2	101.0	100.1	99.1	100.3	100.0	98.5	99.0	99.4	99.2	100.4
Xception-65	100.0	100.0	100.0	100.0	100.0	100.0	100.0	100.0	100.0	100.0	100.0	100.0	100.0	100.0	100.0	100.0	100.0	100.0
w/o ASPP	102.7	102.6	101.0	101.5	103.5	104.0	103.7	103.2	103.6	103.2	102.8	103.4	104.2	103.2	103.3	103.8	103.5	100.8
w/o AC	100.9	101.0	100.4	100.8	99.4	98.7	100.1	100.9	101.1	101.6	100.2	101.3	101.2	101.0	100.7	101.3	100.7	100.9
w/ DPC	99.6	100.3	100.7	99.9	100.2	101.3	100.1	100.2	99.6	100.6	100.6	101.1	100.4	100.2	99.6	100.7	100.6	99.9
w/o LRL	100.3	100.2	100.4	100.0	98.6	100.1	98.8	99.2	99.6	100.5	100.1	101.1	100.6	99.9	100.2	101.0	99.3	99.3
w/ GAP	99.4	99.4	99.7	99.2	98.0	98.8	98.3	98.6	98.7	99.9	99.6	99.7	100.1	99.3	99.3	99.3	97.9	99.5
Xception-71	100.0	100.0	100.0	100.0	100.0	100.0	100.0	100.0	100.0	100.0	100.0	100.0	100.0	100.0	100.0	100.0	100.0	100.0
w/o ASPP	103.3	103.1	102.6	102.6	104.3	104.6	104.3	104.6	104.5	103.8	103.8	103.9	103.6	103.8	104.4	103.6	104.1	103.0
w/o AC	100.2	101.4	100.0	100.4	100.0	100.5	100.6	101.8	101.8	101.7	102.8	101.3	101.5	100.5	101.5	102.1	100.1	102.1
w/ DPC	101.4	100.8	101.4	101.0	100.7	101.8	101.2	101.4	100.9	101.1	101.7	101.3	100.7	100.4	101.5	101.1	101.5	101.3
w/o LRL	101.9	100.7	101.0	100.6	103.0	102.0	103.0	102.9	102.1	101.3	101.5	101.9	101.1	101.3	101.0	101.0	100.2	101.1
w/ GAP	100.5	99.7	100.5	99.9	100.5	100.6	100.8	101.1	101.5	100.2	100.4	100.8	100.1	99.3	100.1	99.6	98.6	101.3

Table B.9: CD for corrupted variants of the validation set of ADE20K for several network backbones of the DeepLabv3+ architecture and respective architectural ablations. Highest CD per corruption is bold.

	Blur				Noise					Digital				Weather				Geometric Distortion
Deeplab-v3+ Backbone	Motion	Defocus	Frosted Glass	Gaussian	Gaussian	Impulse	Shot	Speckle	Intensity	Brightness	Contrast	Saturate	JPEG	Snow	Spatter	Fog	Frost	
MobileNet-V2	100.0	100.0	100.0	100.0	100.0	100.0	100.0	100.0	100.0	100.0	100.0	100.0	100.0	100.0	100.0	100.0	100.0	100.0
w/o ASPP	82.3	88.6	85.4	86.6	79.5	77.4	78.9	80.2	83.8	74.0	83.8	81.9	82.9	81.0	74.5	88.0	82.0	74.2
w/o AC	100.1	99.4	98.9	99.6	100.0	96.5	100.2	102.4	105.5	91.8	100.9	105.0	92.8	97.7	93.3	100.0	96.7	95.0
w/ DPC	97.2	91.7	99.2	95.5	95.1	93.4	96.4	95.5	94.9	88.5	97.8	93.2	95.0	99.2	90.7	94.8	98.5	93.2
w/o LRL	98.5	96.7	99.4	97.5	93.6	96.3	93.8	94.5	95.7	97.7	99.3	106.0	97.7	98.6	93.8	98.1	97.1	99.6
w/ GAP	99.0	97.8	102.8	100.9	101.7	97.9	101.7	105.0	101.4	94.0	102.8	99.3	94.6	99.8	91.4	101.0	99.3	100.9
ResNet-50	100.0	100.0	100.0	100.0	100.0	100.0	100.0	100.0	100.0	100.0	100.0	100.0	100.0	100.0	100.0	100.0	100.0	100.0
w/o ASPP	83.1	89.8	88.1	89.0	79.6	79.7	78.6	78.6	90.9	77.6	84.5	85.4	87.9	80.2	79.9	89.8	83.1	92.4
w/o AC	94.1	97.4	97.4	97.8	98.0	100.1	98.9	97.8	101.1	100.0	99.0	100.4	99.0	99.9	101.6	98.0	99.6	114.1
w/ DPC	98.0	99.6	99.8	100.0	105.0	104.5	105.5	103.9	99.8	100.5	98.1	103.8	98.9	102.3	107.0	99.4	102.1	108.3
w/o LRL	94.3	95.1	100.0	98.4	98.8	99.4	99.2	98.0	103.8	88.5	90.4	88.3	92.4	99.6	97.1	91.4	97.6	102.4
w/ GAP	97.3	97.1	102.9	100.8	97.6	103.2	97.6	94.1	88.1	84.4	96.4	89.5	93.5	98.9	94.7	91.8	98.0	113.9
ResNet-101	100.0	100.0	100.0	100.0	100.0	100.0	100.0	100.0	100.0	100.0	100.0	100.0	100.0	100.0	100.0	100.0	100.0	100.0
w/o ASPP	86.3	94.7	86.3	90.3	76.9	80.3	75.8	74.7	77.9	74.6	88.3	86.3	98.5	83.9	80.6	95.7	83.2	86.1
w/o AC	99.9	99.1	98.2	99.8	100.8	97.1	100.8	102.7	104.5	90.1	103.8	102.8	101.3	99.9	94.4	101.4	98.2	96.8
w/ DPC	94.8	94.8	96.0	96.3	95.7	95.6	94.7	92.4	96.1	85.5	98.6	89.1	96.8	100.1	94.2	97.8	98.3	95.4
w/o LRL	98.0	97.1	95.6	96.4	92.6	97.6	92.6	91.3	90.8	91.2	96.5	98.6	110.6	99.6	101.1	93.0	97.6	101.6
w/ GAP	100.5	100.0	102.6	101.6	103.1	106.2	103.2	102.9	99.6	92.8	102.3	92.9	95.6	102.3	104.8	98.2	98.1	96.4
Xception-41	100.0	100.0	100.0	100.0	100.0	100.0	100.0	100.0	100.0	100.0	100.0	100.0	100.0	100.0	100.0	100.0	100.0	100.0
w/o ASPP	90.8	90.3	90.2	89.8	91.4	88.7	91.1	91.9	104.6	92.7	93.8	95.5	100.7	90.7	86.6	105.6	92.3	77.0
w/o AC	94.0	95.1	92.5	94.1	87.8	92.9	89.7	90.1	92.1	90.7	97.7	92.2	90.2	98.0	92.5	106.1	98.7	101.4
w/ DPC	104.3	104.2	102.2	102.6	106.1	105.4	107.6	109.5	116.2	98.5	106.0	105.5	103.4	99.0	100.1	118.5	100.2	108.8
w/o LRL	100.0	96.9	98.0	97.4	96.5	99.5	96.5	94.2	107.8	89.9	95.6	97.0	97.1	94.7	92.8	105.9	97.3	91.7
w/ GAP	92.8	94.4	96.6	95.1	90.7	95.1	90.4	91.3	100.1	88.6	92.6	93.8	90.9	92.5	90.3	90.2	94.0	92.7
Xception-65	100.0	100.0	100.0	100.0	100.0	100.0	100.0	100.0	100.0	100.0	100.0	100.0	100.0	100.0	100.0	100.0	100.0	100.0
w/o ASPP	104.3	103.8	97.9	99.3	107.8	108.8	108.5	107.5	117.5	113.6	104.9	114.0	120.2	105.3	108.0	112.2	106.6	86.3
w/o AC	96.0	95.8	95.1	95.8	89.8	88.7	92.8	94.7	88.5	92.3	92.8	91.9	91.8	98.0	93.3	95.6	96.3	86.2
w/ DPC	95.4	98.3	100.0	96.9	97.9	102.6	97.6	97.1	86.7	97.4	99.8	102.8	96.7	98.7	94.1	100.0	99.8	90.3
w/o LRL	98.6	97.9	99.2	97.5	91.4	98.0	92.2	92.6	88.2	97.0	97.6	103.0	98.5	97.9	97.5	101.6	95.4	83.7
w/ GAP	98.6	98.6	99.7	97.7	92.7	96.6	94.2	94.4	89.7	102.8	99.6	100.4	104.0	98.7	97.9	97.6	93.5	97.7
Xception-71	100.0	100.0	100.0	100.0	100.0	100.0	100.0	100.0	100.0	100.0	100.0	100.0	100.0	100.0	100.0	100.0	100.0	100.0
w/o ASPP	103.6	102.7	101.1	100.8	107.6	108.3	107.8	109.9	118.3	110.7	106.0	110.5	106.5	105.3	109.8	105.8	106.6	101.7
w/o AC	97.1	102.1	97.0	98.0	96.2	98.7	98.9	104.1	108.0	107.2	108.3	102.6	103.7	99.2	103.0	107.0	97.3	112.2
w/ DPC	106.0	103.9	105.1	104.4	103.2	106.7	105.1	107.0	110.6	113.7	107.4	112.5	106.1	101.4	108.2	107.2	105.5	115.9
w/o LRL	106.5	101.7	102.3	101.0	110.7	105.9	110.4	112.4	118.5	110.3	104.8	114.1	105.5	103.0	103.5	103.7	99.4	107.3
w/ GAP	99.7	96.1	100.0	97.3	100.0	100.3	100.9	102.3	109.8	94.5	99.5	101.6	95.4	96.1	97.3	93.8	93.2	107.4

Table B.10: Relative CD for corrupted variants of the validation set of ADE20K for several network backbones of the DeepLabv3+ architecture and respective architectural ablations. Highest rCD per corruption is bold.